NOAA Technical Report NWS 52

Physically-Based Modifications to the Sacramento Soil Moisture Accounting Model:

Modeling the Effects of Frozen Ground on the Rainfall-Runoff Process

Victor Koren
Michael Smith
Zhengtao Cui
Brian Cosgrove

July 2007

U.S. DEPARTMENT OF COMMERCE
National Oceanic and Atmospheric Administration
National Weather Service

A partial listing of recent reports in this series

NWS 50 Distributed Modeling: Phase 1 Results. Michael Smith, Victor Koren, Bryce Finnerty, Dennis Johnson. February, 1999

NWS 51 NOAA NWS Distributed Hydrologic Modeling Research and Development. Michael Smith, Victor Koren, Ziya Zhang, Seann Reed, Dongjun Seo, Fekadu Moreda, Vadim Kuzmin, Zhengtao Cui, Richard Anderson. April, 2004

Physically-Based Modifications to the Sacramento Soil Moisture Accounting Model:

Modeling the Effects of Frozen Ground on the Runoff Generation Process

Victor Koren[1,*], Mike Smith[1], Zhengtao Cui[1, 2], and Brian Cosgrove[1]

[1]Office of Hydrologic Development
NOAA National Weather Service
[2]LEN Technologies

Office of Hydrologic Development
NOAA National Weather Service
1325 East West Highway
Silver Spring, Maryland 20901
victor.koren@noaa.gov
Tel: 301-713-0640 ext. 114
Fax: 301-713-0963

This page intentionally left blank

Preface

This report presents a compilation of research and operational development performed over a multi-year period beginning in 2000[1]. We modify the Sacramento Soil Moisture Accounting (SAC-SMA) model, used by the NOAA National Weather Service for operational river and flash flood forecasting, to include a physically–based representation of the effects of freezing and thawing soil on the runoff generation process. This model is called the SAC-SMA Heat Transfer model (SAC-HT). The frozen ground physics are taken from the Noah land surface model which serves as the land surface component of several National Center for Environmental Prediction (NCEP) numerical weather prediction models. SAC-HT requires a boundary condition of the soil temperature at the bottom of the soil column (a climatic annual air temperature is typically used, and parameters derived from readily available soil texture data. A noteworthy feature of SAC-HT is that the frozen ground component needs no parameter calibration.

SAC-HT was tested at 11 sites in the U.S. for soil temperature, one site in Russia for soil temperature and soil moisture, 8 basins in the upper Midwest for the effects of frozen-ground on streamflow, one location for frost depth, and 75 basins within the Oklahoma Mesonet domain for soil moisture. High correlation coefficients for simulated soil temperature at 3 depths at 11 stations were achieved. Multi-year simulations of soil moisture and soil temperature agreed very well at the Valdai, Russia test location. In eight basins affected by seasonally frozen soil in the upper Midwest, SAC-HT provided improved streamflow simulations compared to SAC-SMA when both models used *a priori* parameters. Further improvement was gained through calibration of the non-frozen ground *a priori* parameters. Frost depth computed by SAC-HT compared well with observed values in the Root River basin in Minnesota, and multi-year soil moisture simulations for 75 basins in the Oklahoma Mesonet domain were equal to, or better than, those from the Noah and Mosaic land surface models.

Our work uncovered a deficiency in the SAC-SMA and SAC-HT models regarding the drying of the soil layers due to evapotranspiration. In an attempt to resolve this deficiency, *a priori* SAC-HT non-frozen ground model parameters were adjusted over the Conterminous United States (CONUS). However, even with the adjusted parameters, SAC-HT still over-predicted the drying of the lower soil layer. In a companion report, we address this deficiency by adding a physically-based treatment of evapotranspiration to the SAC-HT.

1. Introduction and Statement of Problem

The National Weather Service (NWS) of the National Oceanic and Atmospheric Administration (NOAA) is mandated to produce river and flash flood forecasts for the Nation (McEnery et al., 2005; Carter, 2002). Field forecasters accomplish this mission by using the NWS River Forecast System (NWSRFS; Larson et al., 1995), an end-to-end system that ingests data from numerous sources and ends with the user generating river and flash flood forecasts.

Heat and moisture transfer processes in the soil aeration zone play an important role

[1]The majority of this work was completed as part of OHD Hydrologic Operations and Services Improvement Process (HOSIP) project OHD-2005-029 approved June 27, 2007. Some of the results in this report have been presented at conferences or published in journals.

in the runoff generation mechanism in regions where seasonal soil freezing/thawing occurs. Cold season processes greatly affect the transformation of snow/rain into runoff, in particular the partitioning of precipitation and snowmelt into surface runoff and infiltrating water. A particular manifestation of this problem occurs in the upper Midwest, where shallow snowpack depths and limited vegetation provide little insulation against the extremely low air temperatures that can occur. These are near optimal conditions for deep penetration of frost. In addition, soil moisture saturation is usually very high during cold season. In such cases, water held in the soil layers is frozen, impeding the percolation of liquid water to lower soil layers and creating an impervious surface layer that generates rapid runoff from subsequent rainfall events. Another aspect of this phenomenon is the rise in streamflow in the spring when the frozen soil thaws and releases water into the channel systems. Often, this can occur on non-rainy days, presenting a perplexing modeling and forecasting problem for hydrologists.

Koren et al. (1999) present examples of the effects of frozen ground and we repeat one of them here to illustrate the problem. Figure 1 shows the effects of frozen soil in the Root River basin in Minnesota, where winter temperatures and shallow snow packs can generate frozen soil to a depth of two meters. Two distinct rainfall-runoff relationships can be seen in Figure 1, with the same amount of rain producing much more runoff in the case of frozen ground conditions. The antecedent precipitation index at each point is labeled. The scatter of the soil moisture depths in Figure 1 show that the different rainfall-runoff regimes are not explained by soil moisture depth alone.

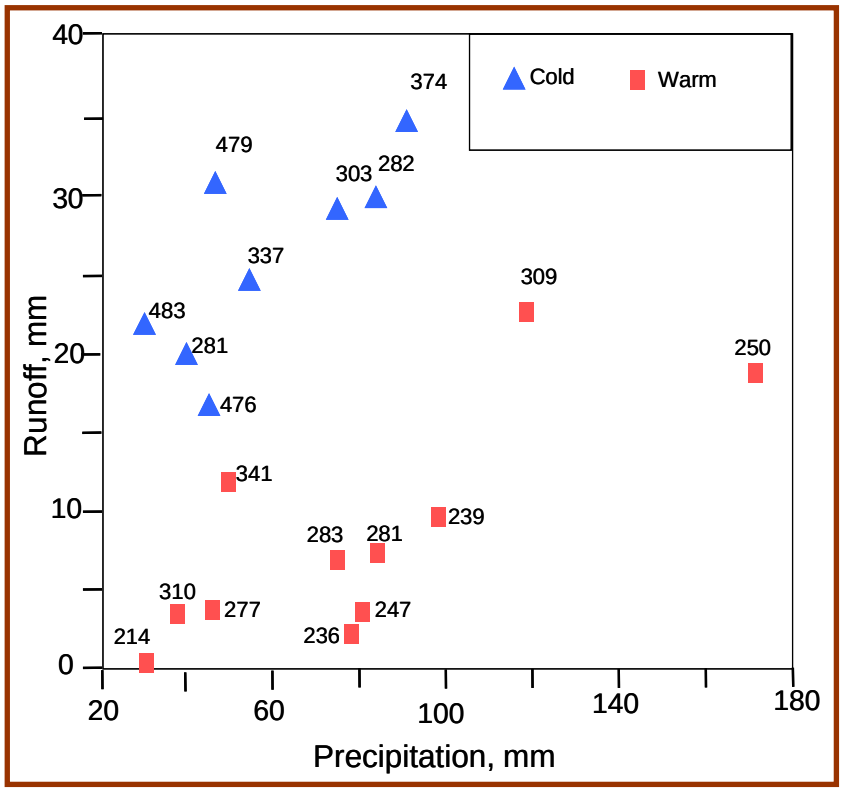

Figure 1. Precipitation-runoff relationship during periods when soil is estimated to be frozen or unfrozen. Points are labeled with antecedent precipitation index in mm. (Adapted from Koren et al., 1999).

X. Zhang et al. (2010) reported that vast geographical regions are impacted by seasonally frozen ground. Land surface models (LSMs) and Soil Vegetation Atmosphere Transfer schemes (SVATs) used for regional scale modeling or coupled with numerical weather prediction models (NWPs) continue to be developed to handle these impacts. For example, Luo et al. (2003) reported the results of 21 LSMs that participated in Phase 2(d) of the Project for Intercomparison of Land-Surface Parameterization Schemes (PILPS 2(d)). One of the specific foci of PILPS 2(d) was the simulation of soil moisture and temperature with and without explicit frozen soil schemes at the Valdai, Russia water balance site. Additionally, Koren et al. (1999) added a physically-based frozen ground scheme to the NOAA National Centers for Environmental Prediction (NCEP) Noah LSM (Chen et al., 1996; Ek et al., 2003) coupled to the Eta mesoscale model. Updated versions of the Noah LSM continue to be used by NCEP in their current operational suite of coupled models.

Beyond LSMs and SVATS, however, Wang et al. (2010) state that with a few exceptions (e.g., Tian et al., 2006; Mou et al., 2008), frozen soil impacts have been largely ignored in distributed hydrologic models used for basin-scale simulations. We believe that even less attention in this regard has been paid to hydrologic models used for *operational* fine-scale streamflow simulation and forecasting. Those hydrologic models that have been modified for frozen soil have additional parameters that require calibration, which impedes their widespread use in operational forecasting (Anderson and Neuman, 1984; Emerson, 1994; Wang et al., 2010).

Our strategy in this work was to combine the structures/algorithms of two successful models: SAC-SMA and the Noah LSM. The goal was to develop a model whose complexity is commensurate with current and near-future operational meteorological forcings and application scales, and one that would not require calibration of the frozen ground component.

Our work illustrates a convergence of hydrologic and land surface models. First, we retain the structure of SAC-SMA as it is the precipitation/runoff model used by NWS field offices to generate river forecasts at over 4,000 points nationwide. Supporting the operational use of SAC-SMA is its good performance in a wide array of validation and intercomparison studies for streamflow simulation. SAC-SMA has been tested at various time steps (e.g., 1-24 hour; Reed et al., 2007) and application modes (lumped and distributed - Smith et al., 2011; Reed et al., 2004), and application scales ranging from regional (e.g., Koren, 2006; Finnerty et al., 1997) to country-wide (Xia et al., 2011a, b; Mitchell et al., 2004). SAC-SMA has proven to effectively model a range of runoff-generation mechanisms and responses. We believe our work has broader implications because, in large part, SAC-SMA has a structure common to many so-called conceptual hydrologic models (Clarke et al., 2011; 2008).

Second, we select the frozen ground physics implemented in the Noah LSM (Koren et al., 1999), as this scheme has proven successful in operational numerical weather modeling (Ek et al., 2003; Mitchell et al., 2002). Hereafter, we refer to this modified version of the SAC-SMA as the SAC Heat Transfer (SAC-HT) model. This paper serves as a foundation for a companion paper on the modification of SAC-HT for the enhanced modeling of evapotranspiration.

The remainder of this paper is organized as follows. First we present a review of pertinent literature to place our work in context. In Section 3, we include a brief discussion of the existing SAC-SMA hydrologic model. Following this, we present a thorough

discussion of the physical basis for the new algorithm. The locations and data for testing SAC-HT are discussed in Section 5. Test results from modeled soil moisture and soil temperature at point, basin, and regional scales are described in Section 5. We complete the paper with sections containing conclusions and recommendations.

2. Literature Review

2.1 Hydrologic model modification for frozen ground effects

While considerable theoretical and laboratory analysis of the physical processes of soil freezing/thawing at a point and over a small area has been available for a century, most watershed models do not consider the effect of frozen soil at all, or use empirical index-type relationships to make runoff adjustments under frozen ground conditions. Utilizing results from field experiments, Koren (1980) developed a conceptual approach based on the spatial extent of the frost-induced impermeable layer. He used a gamma distribution of frozen depth and soil moisture to estimate the fraction of impermeable area. A simplified analytical solution was used in the calculation of frozen depth. This parameterization included three empirical parameters which required calibration. Anderson and Neuman (1984) formulated a conceptual modification to SAC-SMA for frozen ground modeling. Their approach first computes a frost index based on air temperature, snow cover (if any), and empirical coefficients for thaw induced by ground heat and water entering the soil. The frost index is then used to reduce the amount of percolation and interflow. As a conceptual model, this approach required the calibration of seven parameters of the frozen ground component. Similarly, Emerson (1994) added modules to the Precipitation Runoff Modeling System (PRMS) model for daily accounting of the heat and water in the soil. This model also required parameter calibration. Wang et al. (2010) added an empirical frozen ground algorithm to a distributed biosphere hydrologic model (SiB2) and tested the model on a 30.5km^2 watershed in China at hourly time steps. Their approach also required the calibration of two parameters.

2.2 LSMs and frozen soil modeling

The development of frozen soil algorithms within LSMs, SVATS, and macroscale hydrologic models has been an active area of research, with numerous schemes being developed over last several decades. Li et al. (2010) present perhaps the first-ever classification of many of these schemes based on the complexity of the governing equations and the processes included. The four levels of model complexity were arranged such that level 1 indicated the most complete modeling approach. Their analysis suggests that simplification of the governing moisture and temperature equations from level 1 to 4 does not lead to a significant reduction in simulation accuracy. More important is the parameterization of the freezing-melting process, with the parameterization derived from the freezing-point depression equation and soil matric potential equation supported by both thermodynamic equilibrium theory and simulation results.

Luo et al. (2003) discuss the results of a comprehensive evaluation of 21 snow/frozen soil models in PILPS 2(d). They noted that the impact of frozen ground on soil moisture was inconclusive due to the particular climate conditions at the site (soil moisture near saturation

with little variability during the snowmelt period). However they found that those models that explicitly accounted for frozen ground effects featured improved simulation of soil temperature at seasonal to interannual time scales.

Several LSMs containing frozen ground schemes have participated in hydrologic modeling studies and are worth mentioning here. Given the realization that the inclusion of soil temperature and the related effects on sensible and latent heat improved weather forecasts, Cherkauer and Lettenmaier (1999) modified the macroscale Variable Infiltration Capacity two-Layer (VIC-2L) model of Liang et al. (1996) to include frozen soil and snow physics. The VIC model is unique among LSMs/SVATS due to its additional focus on runoff generation. Their goal was to include such physics at a level of complexity commensurate with the previously developed VIC model. Cherkauer et al. (2003) further modified the VIC-2L frozen soil physics to account for permafrost and spatially distributed seasonal soil frost. VIC-2L was used in phase 1 of the Distributed Model Intercomparison Project (Reed et. al., 2004) for hydrologic simulation at operational basin scales. Unfortunately, the VIC-2L model was run at a daily time step in DMIP 1 instead of the required hourly time step, so detailed evaluations of the VIC-2L simulations were not possible.

3. Development of SAC-HT

3.1 Overview of original SAC-SMA model structure

A detailed description of SAC-SMA can be found in Burnash et al. (1973). The basic design of the SAC-SMA model centers on a two-zone structure: a relatively shallow upper zone, and a (typically) much thicker lower zone which supplies moisture to meet the evapotranspiration demand. There is no direct connection of these zones to soil profile properties. Rather, the depths of the zones are treated as model parameters. Each zone consists of tension and free water storages that interact to generate five runoff components and tension water, $S_{t,i}$, and free water, $S_{f,i}$, soil moisture states (later in Figure 4 we use acronyms *UZTWC, UZFWC, LZTWC, LZFSC,* and *LZFPC* for these states). The free water storage of the lower zone is divided into two sub-storages which control supplemental (fast) base flow and primary (slow) ground water flow. The partitioning of rainfall into surface runoff and infiltration is governed by the upper zone soil moisture states and the percolation rate to the lower zone. In general, no runoff occurs until the tension water capacity of the upper zone is filled. After that, surface runoff generation is controlled by the content of the upper zone free water storage and the deficiency of lower zone tension and free water storages. Each of three free water reservoirs can generate runoff q depending on a depletion coefficient of the reservoir:

$$q_i = r_i \cdot S_{f,i} / \Delta t \qquad (1)$$

It is assumed that the free water reservoirs, $S_{f,i}$, are linear with constant depletion coefficients, r_i. Index i ranges from one to three and refers to the single upper zone and two lower zone free water storages, and Δt is the time interval.

The percolation rate into the lower zone is a nonlinear function of the saturation of

the lower and upper zone free water reservoirs:

$$I_{perc} = \left[I_o + I_{\max} \cdot (1 - \frac{S_{t,2} + S_{f,2} + S_{f,3}}{S_{t\max,2} + S_{f\max.2} + S_{f\max,3}})^{\beta} \right] \frac{S_{f,1}}{S_{f\max,1}} \qquad (2)$$

where I_o is the minimum percolation rate under fully saturated conditions in the upper and lower layers, $I_o = S_{f,2} \cdot r_2 + S_{f,3} \cdot r_3$, I_{max} is the maximum percolation rate, β is an exponent value that controls the shape of the percolation curve, and $S_{tmax,i}$ and $S_{fmax,i}$ are tension water and free water storage capacities, respectively. Water which percolates into the lower zone is divided among the three storages of the zone based on the sizes of the storages and their current states.

3.2. Frozen ground physics implementation strategy

Heat and moisture transfer processes in the soil aeration zone play an important role in the runoff generation mechanism in regions where seasonal soil freezing/thawing occurs. One challenge is that the conceptual representation of a soil profile in commonly used watershed models complicates the implementation of physically-based heat-moisture transfer models that require numerical integration over the soil profile. A second challenge is the formulation of the effects of frozen ground on water fluxes, specifically the partitioning of meltwater/rainfall into surface runoff and infiltration. In watershed modeling, simplified approaches such as empirical equations of the percolation reduction or water balance-type approaches are typically used. The latter assumes that the percolation reduction depends only on frozen water-induced soil porosity reduction. However, field and experimental data suggest that an increase in the surface contact between solid particles and soil water may also be a factor (Kulik, 1969).

We present a physically-based parameterization that addresses the two challenges mentioned above: 1) modification of the storage-type SAC-SMA model to be compatible with the theoretical heat transfer model, and 2) parameterization of frozen ground effects on runoff. The latter is derived from Kozeny's theory (Kozeny, 1927) which accounts for changes in the contact area of solid particles 'free' porosity.

The basic algorithm consists of two main parts. First, the SAC-SMA model is modified to include the effects of frozen soil on the generation of runoff. Second, a physically-based heat transfer component is used to determine the distribution of heat and liquid/frozen water in a soil column. Each part will be discussed in turn.

3.2.1 Modifying the SAC-SMA model to include the effects of frozen soil on the generation of runoff

SAC-HT is intended for operational use at NWS River Forecast Centers (RFCs). Thus, the level of algorithm complexity was constrained by the current use of the typical RFC forcings of precipitation, temperature, and potential evapotranspiration. There is no energy-based computation of skin temperature as in the approach of Koren et al. (1999). Instead, the skin temperature at the snow surface is assumed to be equal to the air temperature. In non-snow areas, the skin temperature of the soil surface is also assumed to

be equal to the air temperature. The energy balance algorithm used herein falls within a moderate level of complexity (Li et al., 2010), commensurate with the intended application.

3.2.1.1 Hydraulic conductivity adjustment due to frozen ground

The most common formulation representing water fluxes under frozen ground conditions assumes that the reduction of soil moisture conductivity depends only on the ratio of liquid water content (θ_l) to soil saturation (θ_s), e.g.:

$$K_f = K_o \cdot \mathrm{f}(\frac{\theta_l}{\theta_s}) \tag{3}$$

where K_f is the saturated hydraulic conductivity adjusted for frozen ground effects and K_0 is the saturated hydraulic conductivity. In this formulation, liquid water content is used instead of total water content but K_0 is assumed to be the same value for frozen and unfrozen soil. However, field and experimental data suggest that an increase in the contact surface between solid particles and soil water is a bigger factor (Kulik, 1969). To account for this additional frozen ground effect on K_0, we use Kozeny's classic theory (Kozeny, 1927) which relates the filtration rate and the soil particle–water contact surface, S_0:

$$K_o = A\frac{\theta_s^3}{S_o^{\ 2}} \tag{4}$$

where A is a parameter that depends on soil properties.

Following Kulik (1969), we assume that the increase in the contact surface due to ice crystals equals $a\theta_f$, where a is the increase in ice crystal surface area per unit of ice content, and θ_f is the ice content. By including this additional contact surface in Equation 4 and dividing the resulting equation by Equation 3, one can obtain an analytical formulation of this effect on the saturated hydraulic conductivity of the frozen ground:

$$K_{o,f} = K_o \frac{1}{[1+(a/S_o)\theta_f]^2} \tag{5}$$

and

$$K_f = K_{o,f} \cdot f(\frac{\theta_l}{\theta_s}) \tag{6}$$

where $K_{o,f}$ is the saturated hydraulic conductivity of frozen ground. Experimental data suggest that the value of a/S_0 does not vary significantly for different soils, and a value of eight is its reasonable estimate. It can be seen from Equations 5 and 6 that the hydraulic conductivity can be reduced considerably due to the change in the surface contact in addition to the liquid water ratio. Figure 2 shows the reduction in hydraulic conductivity as a function of the percentage of ice content.

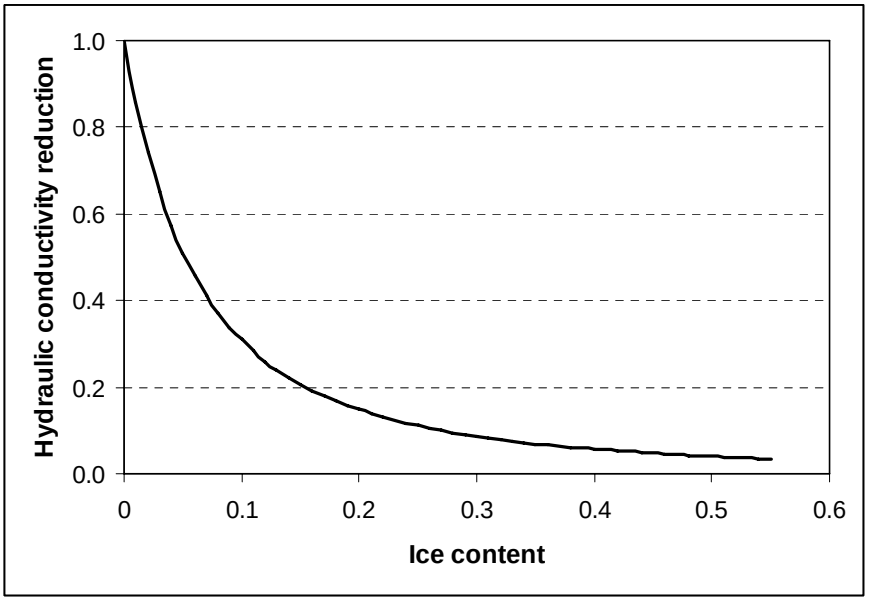

Figure 2. Reduction in saturated hydraulic conductivity due to ice effect on the contact surface between solid particles and soil water.

The effect of frozen ground on the runoff mechanism can vary significantly for different soil types. Koren (2006) performed different tests on the frozen ground effect that support this observation. A plot from Koren (2006) is reproduced here in Figure 3, showing the response of the soil layers to a precipitation event in April, 1965. The left side of Figure 3 shows the impact of accounting for both the soil particle-water contact surface and the volumetric liquid water changes. The right side of the figure shows the impacts of only the volumetric liquid water changes. While percolation decreases and surface runoff increases due to frozen soil conditions over all soil types, finer soils with a significant clay fraction are affected the most. Sandy soils are only slightly affected, even under very wet conditions. Figure 3 also suggests that even under similar frozen conditions, the solid particle-water contact surface is a much bigger factor than just the changes in volumetric liquid water (compare left and right panels of Figure 3).

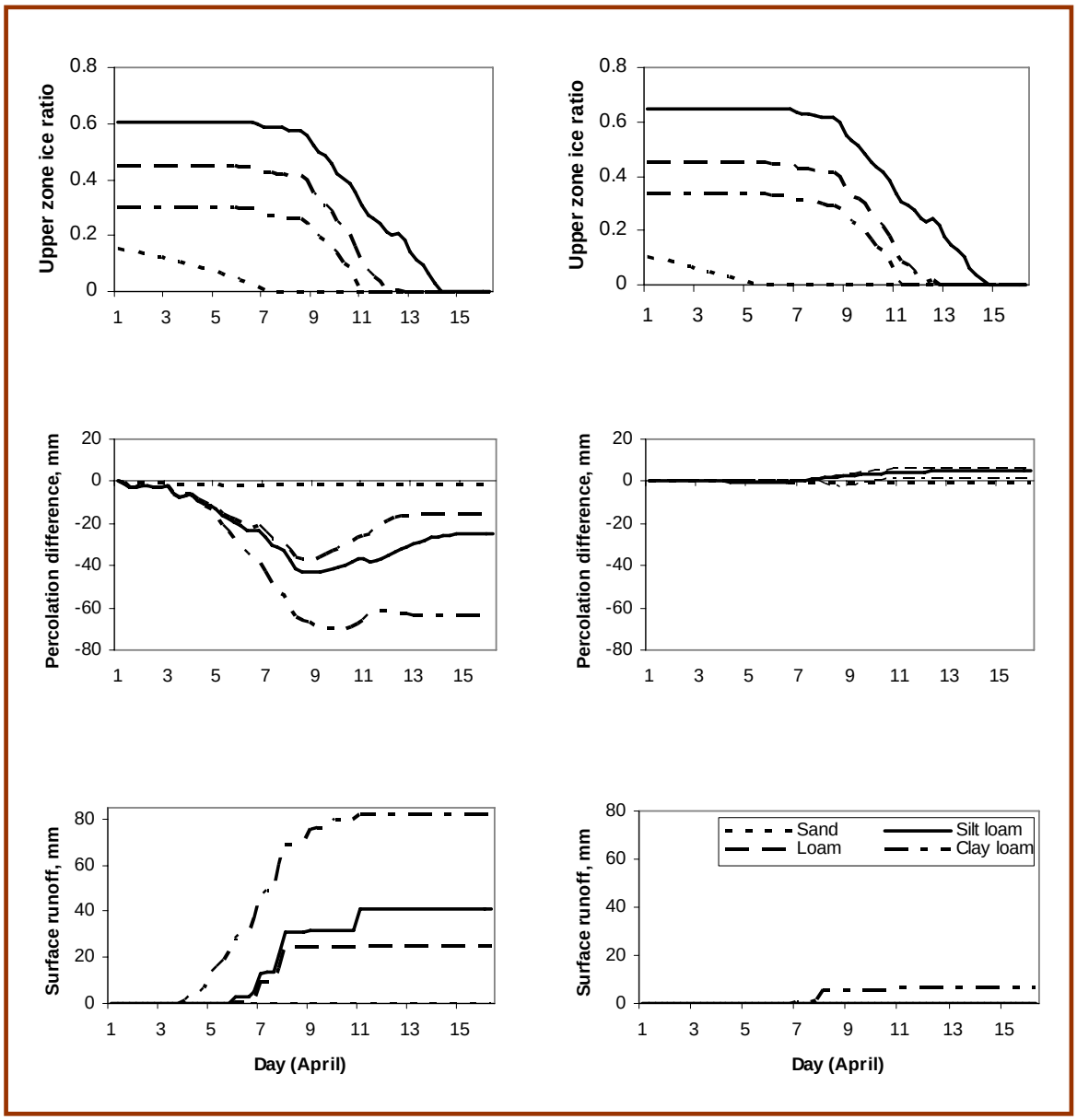

Figure 3. Effect of soil type on frozen ground runoff processes when surface contact and saturation effects are accounted for (left panels), and when only the saturation effect is accounted for (right panels) (Adapted from Koren, 2006).

3.2.1.2 Runoff and percolation adjustment

As mentioned in Section 3.1.1, the original SAC-SMA model runoff components are formulated as linear reservoirs S_i with constant withdrawal rates r_i. The withdrawal rates can be expressed as a function of the hydraulic conductivity $K_{0,i}$ assuming that groundwater level changes are small compared the total depth of groundwater:

$$q_i = r_i \cdot S_i / \Delta t = S_i \cdot (1 - e^{-\alpha_i \cdot \Delta t \cdot K_{0,i}}) / \Delta t \qquad (7)$$

where q_i is the flow from reservoir i, α_i is a constant that depends on soils and topography

properties, and Δt is the time interval. The ratio of the hydraulic conductivity (from Equation 5) to the hydraulic conductivity of unfrozen soil, $K_{0,i}$, is applied to Equation 7 to adjust for the frozen ground effect. The resulting dependency between the original SAC-SMA zone withdrawal rate and frozen ground adjusted rate is:

$$r_i^* = 1 - (1 - r_i)^{(1+8\cdot\theta_f)^{-2}} \tag{8}$$

where the term $(1 + 8 \cdot \theta_f)$ accounts for the increased area between soil particles and liquid water due to ice, with the factor 8 being recommended by Kulik (1978). Appendix A presents the derivation of Equation 8. Koren et al. (2000) derived withdrawal rates of unfrozen soils over the Conterminous United States (CONUS). Equation 8 allows for a simple adjustment to perform simulations under frozen ground conditions. The adjustment is applied to the interflow and fast ground water runoff components as well as to percolation into the lower zone. We assume that the slow ground water component from the deeper soil layer is not directly affected by this factor.

3.2.2 Heat Transfer Component

3.2.2.1 Overview

Modeling the heat transfer process in a column of soil is usually based on a numerical integration of the heat transfer equation over a number of selected soil layers. Two scientific hurdles were overcome to develop a scheme suitable for SAC-SMA. First, the SAC-SMA model does not contain an explicit definition of soil layers. Rather, it defines upper and lower tension and free water storages that could be transformed into a number of soil layers. This hurdle was overcome by recalculating SAC-SMA storage depths into their representative soil layers (described in 3.2.2.2). SAC-SMA storages, represented as totals of tension and free water, plus water content below the wilting point, are recalculated into the required number of soil layers using soil texture data. Three to four layers are usually used with much higher vertical resolution in the upper zone. At each time step, SAC-SMA liquid water storage changes due to rainfall/snowmelt are estimated and then transformed into the soil moisture states of the heat transfer model. The heat transfer model splits the total water content into frozen and liquid water portions based on a simulated soil temperature profile (section 3.2.2.3). Estimated new soil moisture states are then converted back into the SAC-SMA model storages as shown in Figure 4. The time step of the frozen ground component may be a fraction of the SAC-SMA time step.

The second hurdle to be overcome was that the heat transfer component requires the depth of snow above the soil surface in order to compute the soil surface temperature. To meet this need, the NWS snow accumulation and melt model (Snow-17, Anderson, 2006; 1976) was modified to compute time series of snow depth. Time series of computed snow depth are also useful for the calibration of Snow-17, as there are many observations of snow depth. Where there is no snow pack, the soil surface temperature is assumed to be equal to the air temperature.

3.2.2.2 Conversion of SAC-SMA zones to physical soil layers

We derived an approach to convert the SAC-SMA conceptual storage layer depths to physically-based layers using soil texture information. Figure 4 illustrates this conversion. Koren et al. (2000; 2003) developed a set of relationships that link SAC-SMA storages (parameters) and soil properties such as porosity, field capacity, wilting point, and hydraulic conductivity. They assumed that tension water storages of the SAC-SMA model are related to available soil water, and that free water storages are related to gravitational soil water.

The model parameter-soil property relationships allow for recalculating the upper and lower SAC-SMA soil moisture capacities into soil moisture contents in a number of physical soil layers as shown in Figure 4. The SAC-HT begins with a default of five physical soil layers. Thinner layers are used closer to the soil surface. However, the default number of soil layers and their thicknesses are automatically adjusted using SAC-SMA parameter values at the selected location upon the execution of the model. A variable number of soil layers can be assigned in this approach similar to Koren et al. (1999), which simplifies its coupling to the SAC-SMA model. The number of soil layers allocated to the upper and lower zones varies depending on gridded SAC-SMA storages and soil properties. To make adjust the default number of layers and their depths, the upper, $\boldsymbol{Z_U}$, and lower, $\boldsymbol{Z_L}$, zone depths of the SAC-HT are estimated first to be sure that the upper and lower SAC-SMA capacities are preserved:

$$Z_U = \frac{S_{t\,\max,1} + S_{f\,\max,1}}{\theta_{s,1} - \theta_{wlt,1}} \tag{9}$$

$$Z_L = Z_U + \frac{S_{t\,\max,2} + S_{f\,\max,2} + S_{f\,\max,3}}{\theta_{s,2} - \theta_{wlt,2}} \tag{10}$$

where $\theta_{s,i}$ and $\theta_{wlt,i}$ are the upper and lower zone saturation soil moisture content and wilting point respectively in m^3/m^3. The default SAC-HT defined layer depths are then adjusted to be consistent with the $\boldsymbol{Z_U}$ and $\boldsymbol{Z_L}$ estimates. Because of this, the number of soil layers may be less than five (e.g., for shallower soils), and can be different for different pixels or basins.

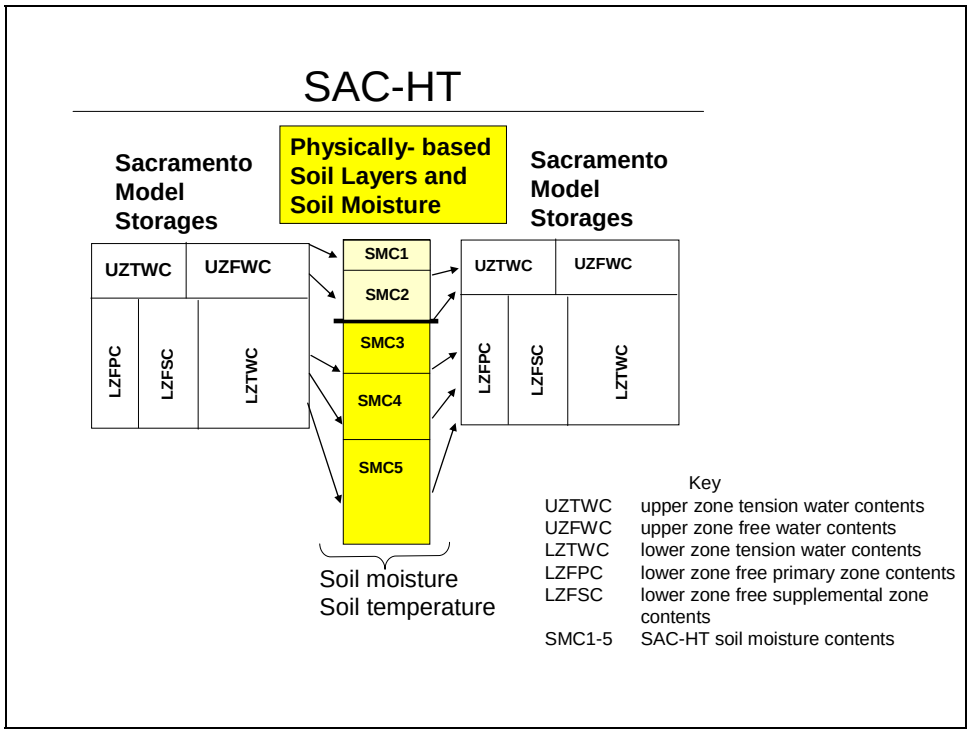

Figure 4. Conversion between Sacramento Model conceptual soil layers and physically-based soil layers performed in SAC-HT. SMC1 and SMC2 represent the upper zone, and SMC3, 4, and 5 represent the physical lower zone.

3.2.2.3 Heat Transfer in the Soil Layers

The basic heat transfer model that accounts for soil moisture phase transitions in Koren et al. (1999) is also used in the formulation of SAC-HT. We repeat the equation here for completeness:

$$c(\theta,\theta_{ice})\frac{\partial T}{\partial t} = \frac{d}{dz}\left[K(\theta,\theta_{ice})\frac{\partial T}{\partial z}\right] + \rho \cdot L\frac{\partial \theta_{ice}}{\partial t} \qquad (11)$$

where c is the volumetric heat capacity, T is soil temperature, K is the thermal conductivity of the soil, θ is the volumetric soil moisture content, θ_{ice} is the volumetric ice content, ρ is the density of water, z is depth, and t is time. The last term of Equation 11 accounts for the soil moisture phase transition. Heat and soil moisture fluxes are simulated separately at each time step, assuming no significant heat transfer during the redistribution of liquid water (Taylor and Luthin, 1976). Li et al. (2010) classify Equation 11 as a level 3 (moderate complexity) approach. The layer-integrated form of Equation 11 is:

$$c\Delta z_i \frac{\partial T_i}{\partial t} = (K\frac{\partial T}{\partial z})_{z_{i+1}} - (K\frac{\partial T}{\partial z})_{z_i} + \rho L \Delta z_i \frac{\partial \theta_{ice,i}}{\partial t} \qquad (12)$$

(12)

where Δz_i is the soil layer thickness, and L is the latent heat of fusion. The liquid water

content depending on soil temperature and soil moisture is estimated from the Clausius-Clapeyron equation for phase equilibrium combined with Campbell's relationship between water potential and water content adjusted for the effects of frozen soil:

$$\frac{g\psi_s}{L}(1+8\cdot\theta_{ice})^2\cdot(\frac{\theta-\theta_{ice}}{\theta_s})^{-b}-\frac{T}{T+273.16}=0 \qquad (13)$$

where θ is the total water content, θ_s is the soil saturation, ψ_s is the soil water potential at saturation, and b is the Campbell's relationship parameter. Equation 13 corresponds to Equation 17 in Koren et al. (1999) and was also adopted by Niu and Yang (2006) and Li et al. (2010).

An implicit Crank-Nicholson scheme is used to solve Equation 12 and an explicit approximation is applied to the source/sink term. During rapid freezing and thawing of soils, Equation 12 is solved twice to reduce numerical error. As discussed previously, to simplify the approach for operational use, near surface air temperature is used in place of skin temperature measurements at the upper boundary. In addition, the long-term mean annual air temperature is used as the lower boundary (usually at a 3m depth).

At each time step, the algorithm estimates the changes in SAC-SMA liquid water storage due to snowmelt and rainfall, and then transforms them into the layered soil moisture states of the heat transfer model. The heat transfer model then splits the total water content into frozen and liquid water portions based on simulated soil temperature profile. These newly estimated soil moisture states are then converted back into the SAC-SMA model storages using the relationships between SAC-SMA storage parameters and soil properties described above.

4. Test Sites and Data

4.1 Overview

Many tests were conducted to evaluate the individual components as well as the overall performance of SAC-HT. Tests were conducted at point, basin, and regional scales. We describe the test sites and data for each testing scenario below.

4.1.1 Point tests of soil temperature and soil moisture

We selected various sites that had seasonally frozen ground for testing SAC-HT. Eleven sites in the upper Midwest and one site in Russia were used for point-type soil column evaluations. Data for the Midwest sites were retrieved from the National Climatic Data Center (NCDC). At the Midwest stations, soil temperatures were measured at multiple depths of 5, 10, 20, 50, and 100 centimeters once per day. Table 1 lists the information for the eleven sites in the U.S. and the single site in Russia, and Figures 5 and 6 show the locations of the sites. The site at Valdai, Russia, has good quality hydrologic and meteorological data for an 18-year period and has been used in multiple studies (e.g., Luo et al., 2003; Schlosser et al., 1997; Vinnikov et al., 1996). At the Valdai experimental site, soil

moisture observations were taken at 12 points within the 0.36km^2 Usadievskiy catchment, usually every 10 days. These observations were the total amount of water in each 10cm layer down to a 100cm depth, (Luo et al., 2003). We used spatial averages of these 12 points as described by Schlosser et al. (1997). Computed and observed soil moisture amounts in the 0-20, 0-50, and 0-100cm layers were compared.

4.1.2 Lumped basin-scale simulations of runoff

In addition to the point-type validation exercises, we tested SAC-HT in eight river basins to examine runoff from seasonally frozen soil. We applied SAC-HT as a lumped model to generate streamflow and soil moisture. Table 2 presents the basins and their characteristics, and Figure 5 shows the locations of the basins. We used mean areal 6-hourly precipitation and air temperature time series derived from data available from NCDC. The time series spanned from 25 to 40 years depending on the basin, the same length of time for which daily discharge values at basin outlets are available from the USGS. We used empirical unit hydrographs to transform basin average simulated runoff into outlet hydrographs.

4.1.3 Regional simulation of soil moisture and soil temperature

Further testing was performed in the region covered by the Oklahoma Mesonet. These tests were specifically designed to evaluate the soil moisture simulations generated by SAC-HT. The Oklahoma Mesonet was created in the early 1990s as an automated state-wide network of meteorological observing stations. The Mesonet consists of over 100 stations, or roughly one station per county as shown in Figure 7. This network was designed to operate in real time, observe nine meteorological variables, transmit these observations in real time, and relay the data to a central site for collection, quality control, and storage for use and dissemination (Illston et al., 2008, 2004; Brock et al., 1995). Soil moisture sensors were installed starting in 1996 at approximately 60 sites, followed by installation at an additional 43 sites in 1998 and 1999 (Schneider et al., 2003; Basara and Crawford, 2000). The sensors provide soil moisture measurements at 5, 25, 60, and 75 cm depths every 30 minutes. In this study, we use daily grids (4x4 km) of soil moisture saturation ratio generated by Koren et al. (2006) from point observations using an inverse distance weighting method. Our analysis grid covers an area slightly larger than the state of Oklahoma and encompasses a wide variety of climatic conditions, ranging from an arid region in the western part to a humid region in the eastern part. The test region features good availability of additional validation data sets needed evaluate SAC-HT. This region has the longest available archive of thoroughly evaluated 4-km NEXRAD-based multi-sensor precipitation grids, and USGS streamflow measurements were available at each of the 70 basin outlets shown in Figure 7.

Table 1. List of stations used in testing SAC-HT

Station Name	NCDC Site ID	Lat	Lon	Elev Above msl (m)	Soil Type (From NCDC)	Simulation Period	Observed Data		
							Max Min Soil Temperature	Daily Max Min Temp	Daily Precipitation
Atlantic, IA	130364	41° 25' N	95° 00' W	353.6	Marshal Silt Loam	1/97-1/02	2, 4, 8, 20, 40 in	Y	Y
Burlington, IA	131060	40° 50' N	91° 10' W	213.4	Grundy Silt Loam	5/97-1/02	2, 4, 8, 20, 40 in	Y	Y
Des Moines, IA	132209	41° 44' N	93° 43' W	292.3	Silty Clay Loam	1/97-4/01	2, 4, 8, 20, 40 in	Y	Y
Estherville, IA	132724	43° 24' N	94° 45' W	402.3	Clarion Silt Loam	1/97-2/01	2, 4, 8, 20, 40 in	Y	Y
Lamoni, IA	134585	40° 37' N	93° 57' W	343.8	Silt Loam	1/97-2/01	2, 4, 8, 20, 40 in	Y	Y
Spencer, IA	137844	43° 10' N	95° 09'W	404.2	Ocheyedan	5/97-1/02	2, 4, 8, 20, 40 in	Y	Y
Toledo, IA	138296	42° 02' N	92° 35' W	289.3	Muscatine Silt Loam	1/97-12/01	2, 4, 8, 20, 40 in	Y	Y
Gaylord, MI	203096	45° 02' N	84° 41'	412.4	Loamy Sand	1/97-12/01	8,20 in	Y	Y
Preston, MN	216654	43° 40' N	92° 04' W	283.5	Clay Loam	1/97-9/00	20 in	Y	Y
Waseca, MN	218692	44° 04'	93° 32' W	351.4	Nicollet Clay Loam	8/98-1/02	2, 4, 8, 20, 40 in	Y	Y
Waubay, SD	398980	45° 25'	97° 20' W	557.8	Sandy Loam	1/97-5/01	2, 4, 8, 20, 40 in	Y	Y
Valdai, Russia	-	58°.0 N	33.2 E	210.0	Silt Loam	7/66-7/83	(Daily) 20, 40 80 cm	Y	Y

Figure 5. Locations of the eleven NCDC stations in the upper Midwest of the U.S. used for point-type soil temperature tests. The locations of the eight test basins are also shown.

Figure 6. Location of the Valdai, Russia meteorological station.

Table 2. River basins used for testing SAC-HT in lumped mode. All are affected by seasonally frozen soil.

River	Drainage area Km 2	USGS Gauge Location	USGS Gauge Number	NWS Basin ID	Lat/Lon
Root River	1593	Lanesboro, MN	05384000	LNEM5	43° 45'N 91° 59'W
Watonwan River	2204	Garden City, MN	05319500	GRDM5	44° 03'N 94° 12'W
Redwood River	671	Marshall, MN	05315000	MMLM5	44° 26'N 95° 51'W
Baldhill Creek	1790	Dazey, ND	05057200	DBCN8	47° 14'N 98° 07'W
Le Sueur River	2849	Rapidan, MN	05320500	RPDM5	44° 07'N 94° 02'W
Lac Qui Parle River	2486	Parle, MN	05300000	LQPM5	44° 60'N 95° 55'W
Long Prairie River	1124	Long Prairie, MN	05245100	LGPM5	45° 58'N 94° 52'W
Rush River	300	Amenia, ND	05060500	AMEN8	47° 01'N 97° 13'W

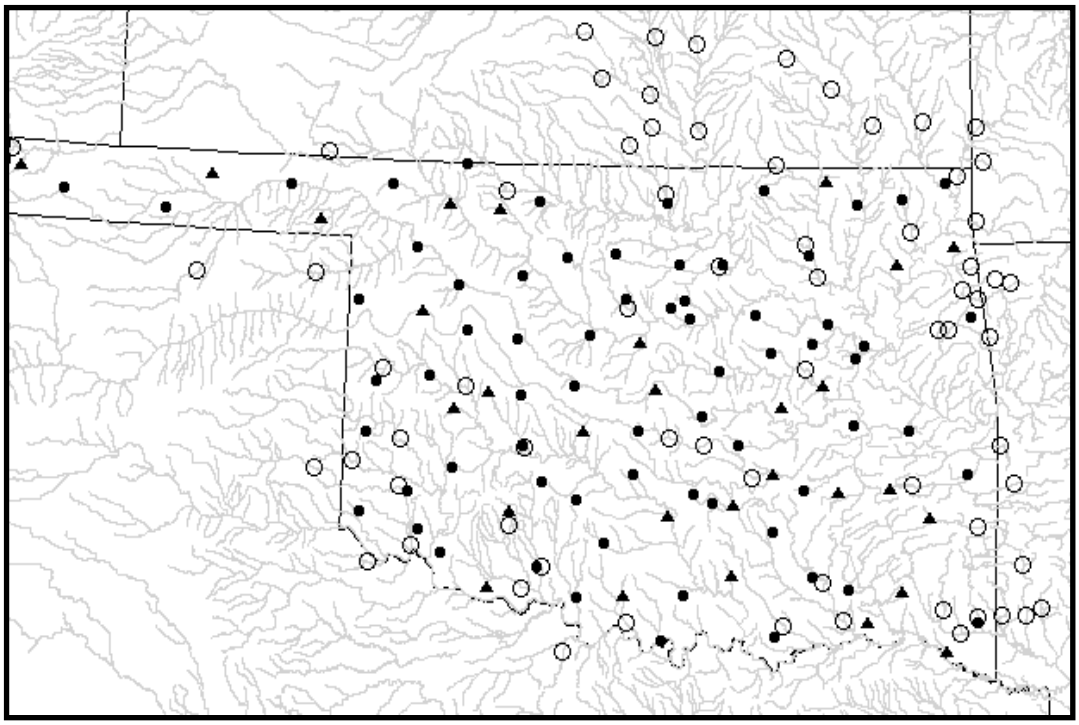

Figure 7. A map of the Oklahoma Mesonet soil moisture sites. Shaded circles are sites with observations in four soil layers; triangles indicate sites with observations at only two top layers; open circles are the outlets of the test basins.

5. Test Results and Discussion

5.1 Point scale tests

SAC-HT was executed at the eleven sites in depicted in Figure 5 and listed in Table 1. Configured with a 0.5hr time step, it generated soil temperature output at levels matching the Mesonet observation depths. Daily precipitation data were retrieved from NCDC, and NCDC max-min daily temperatures were converted to daily temperatures. We used 4km gridded *a priori* SAC-HT model parameters estimated from soil-vegetation data (Koren et al., 2000; 2003) without further calibration. Average daily frozen and liquid soil water content and soil temperature at five layers were produced for 3-5 years depending on the availability of input data.

As shown in Table 3, SAC-HT was able to reproduce the observed soil temperature dynamics very well at all three measurement soil layers. While the correlation coefficients (R) between the simulated and measured soil temperatures are above 0.95, there is a slight decrease in correlation for the top layer. Some of the reduction in the variability of the top layer soil temperature can be explained by the use of daily input forcing data and model time step. Scatter plots of observed and simulated soil temperature for the Des Moines site are shown in Fig. 8. These graphs support this theory, especially at the top soil layer where under-simulated values can be seen at higher soil temperatures when the difference between the maximum and minimum air temperature is usually the greatest. Root mean square error

(RMSE) and Nash-Sutcliffe efficiency (NS, Nash and Sutcliffe, 1970) statistics are also better for the deeper soil layers.

Table 3. Accuracy statistics of simulated soil temperature at three layers: root mean square error (RMSE, in ^{o}C), Nash-Sutcliffe efficiency (NS), and correlation coefficient (R)

Station name	NCDC	5 cm layer			20 cm layer			50 cm layer		
	Site ID	RMSE	NS	R	RMSE	NSE	R	RMSE	NS	R
Lamoni, IA	134585	3.0	0.91	0.96	2.9	0.90	0.99	2.9	0.88	0.99
Atlantic, IA	130364	5.0	0.77	0.96	3.3	0.86	0.99	2.9	0.82	0.98
Burlington, IA	131060	3.3	0.84	0.96	2.5	0.88	0.97	3.0	0.79	0.97
Des Moines, IA	132209	3.7	0.89	0.97	1.9	0.95	0.99	1.6	0.95	0.99
Estherville, IA	132724	4.5	0.83	0.96	2.0	0.95	0.98	2.6	0.88	0.98
Toledo, IA	138296	3.2	0.89	0.97	3.2	0.88	0.98	2.3	0.91	0.99
Preston, MN	216654	3.9	0.87	0.97	2.4	0.91	0.98	2.4	0.87	0.99
Waubay, SD	398980	3.3	0.90	0.96	1.5	0.97	0.99	1.3	0.97	0.99
Spencer, IA	137844	8.1	0.67	0.95	5.1	0.80	0.98	3.6	0.85	0.99
Waseca, MN	218692	-	-	-	-	-	-	3.3	0.87	0.99
Gaylord, MI	203096	-	-	-	3.1	0.86	0.98	2.8	0.84	0.99
Mean		4.2	0.84	0.96	2.8	0.90	0.98	2.5	0.88	0.99

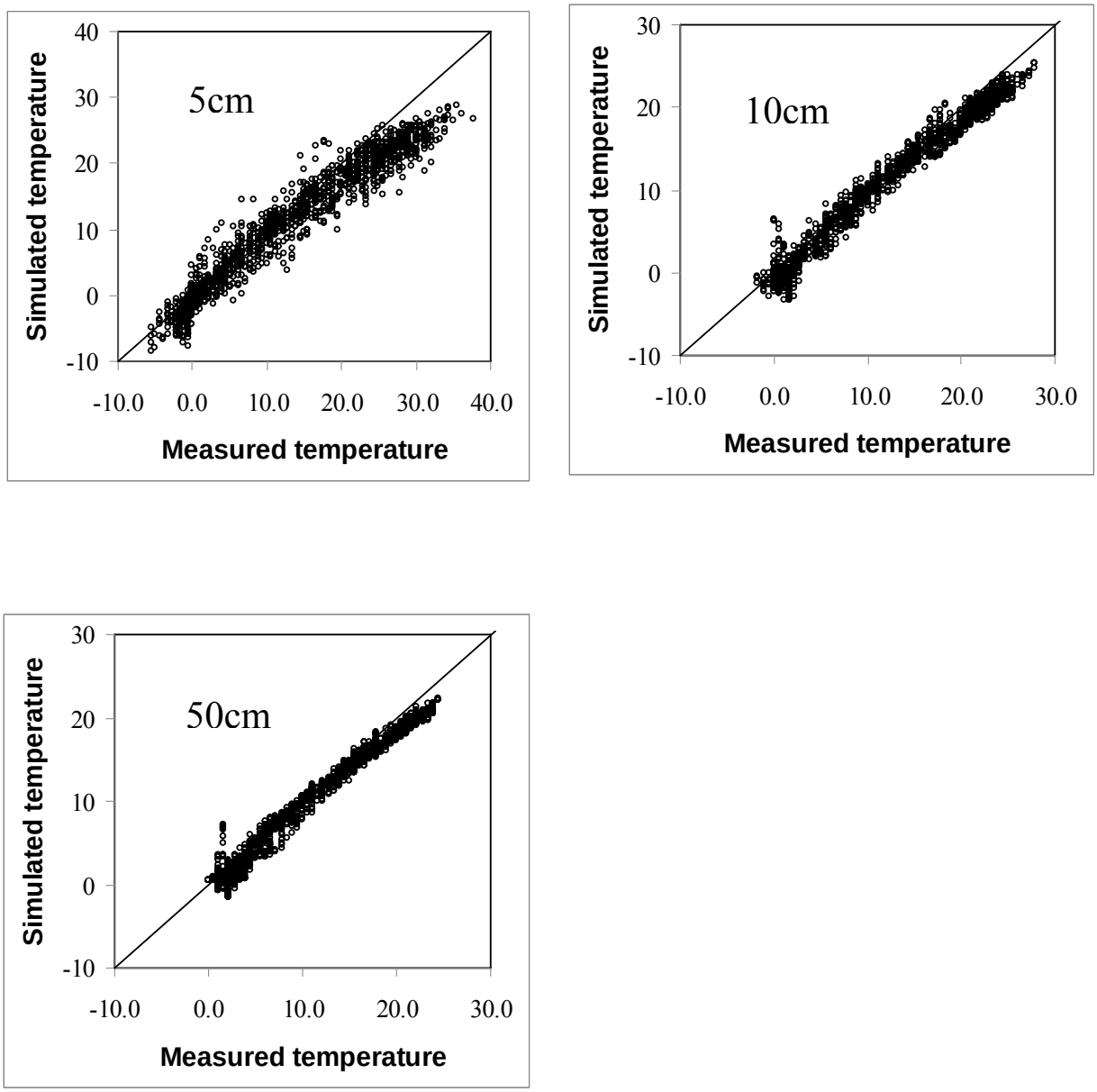

Figure 8. Measured and simulated soil temperature at the Des Moines site for 5, 10, and 50 cm depths (from the top to the bottom panels).

Similar evaluations of SAC-HT were performed for the Valdai, Russia experimental station. We computed total soil moisture amounts in the 0-20, 0-50 and 0-100cm layers to correspond to the Valdai observations. Soil temperatures were computed at 20, 40, and 80cm depths. Figures 9a and 9b show the simulated soil moisture and temperature, respectively, for the 10-year period beginning in 1973. The soil moisture simulations show good agreement with the observations. Our simulations capture the dramatic drying period in the summer of 1975 (Schlosser et al., 1997) in the total 0-100cm layer. Our results agree with those reported in the PILPS experiment at this site (Luo et al., 2003). For example, the shaded areas of Figure 9a show the simulation periods presented in Figures 8 and 9 of Luo et al. (2003). Our results fall within the range of the PILPS model results for the winters of

1975 and 1976. The SAC-HT soil moisture simulation for the 0-100cm layer also agrees well with the two simulations in Figure 15 of Schlosser et al. (1997) and the community land model simulations in Figure 12 of Wang et al. (2008).

In the 0-20cm layer in Figure 9a, our maximum soil moisture contents were limited to about 70mm, while the observed soil moisture were greater. There are several possible reasons for this behavior. First, the computed maximum SAC-HT soil moisture of approximately 70mm is likely due to a fixed value of water holding capacity used in the definition of the SAC-HT soil layers. Other experiments have been impacted by specifying a low value of porosity at Valdai. For example, all models in PILPS underestimated the soil moisture in the 0-10cm layer. Luo et al. (2003) explained that PILPS modelers were required to use the specified total water holding capacity of 40.1cm for the 0-100cm layer (Schlosser et al., 1997), leading to under-simulated soil water values during very wet years. Furthermore, the water table level in Valdai is at fairly shallow depths (Schlosser et al., 1997) and may have entered the top soil layer, making the observed soil moisture greater than the field capacity.

Simulated soil temperatures agree well with Valdai observations as shown in Figure 9b. There seems to be a slight reduction in the amplitude of simulated temperature variability as depth increases. This may be due to the use of a constant thermal conductivity over the entire soil profile. Nonetheless, the simulations in Figure 9 agree well with those from the PILPS 2(d) study (Luo, et al., 2003).

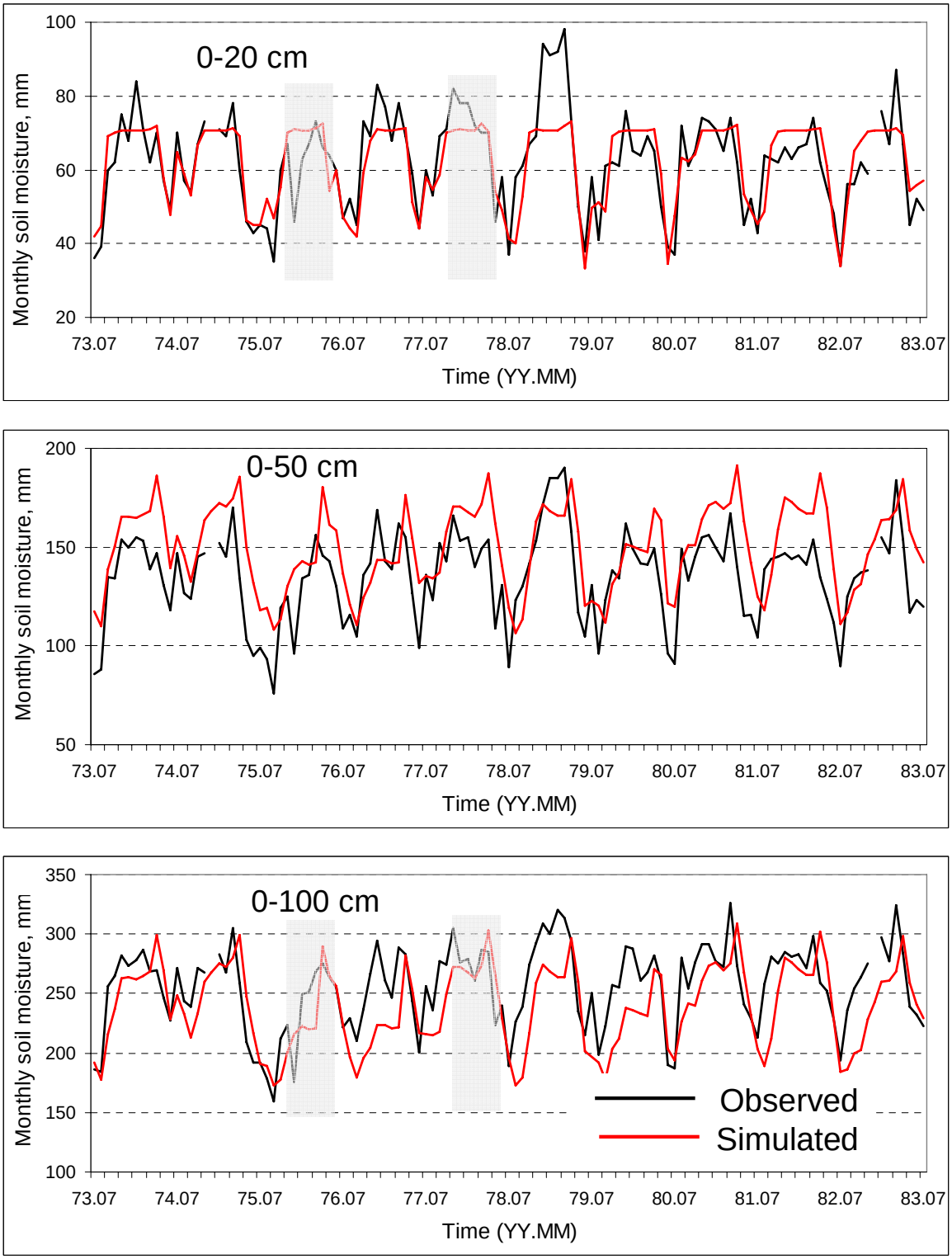

Figure 9a. Simulated and observed soil moisture, Valdai, Russia for three layers: 0-20cm (top), 0-50cm (middle), and 0-100cm (bottom). Shaded areas indicate the period corresponding to Figures 8 and 9 of Luo et al. (2003)

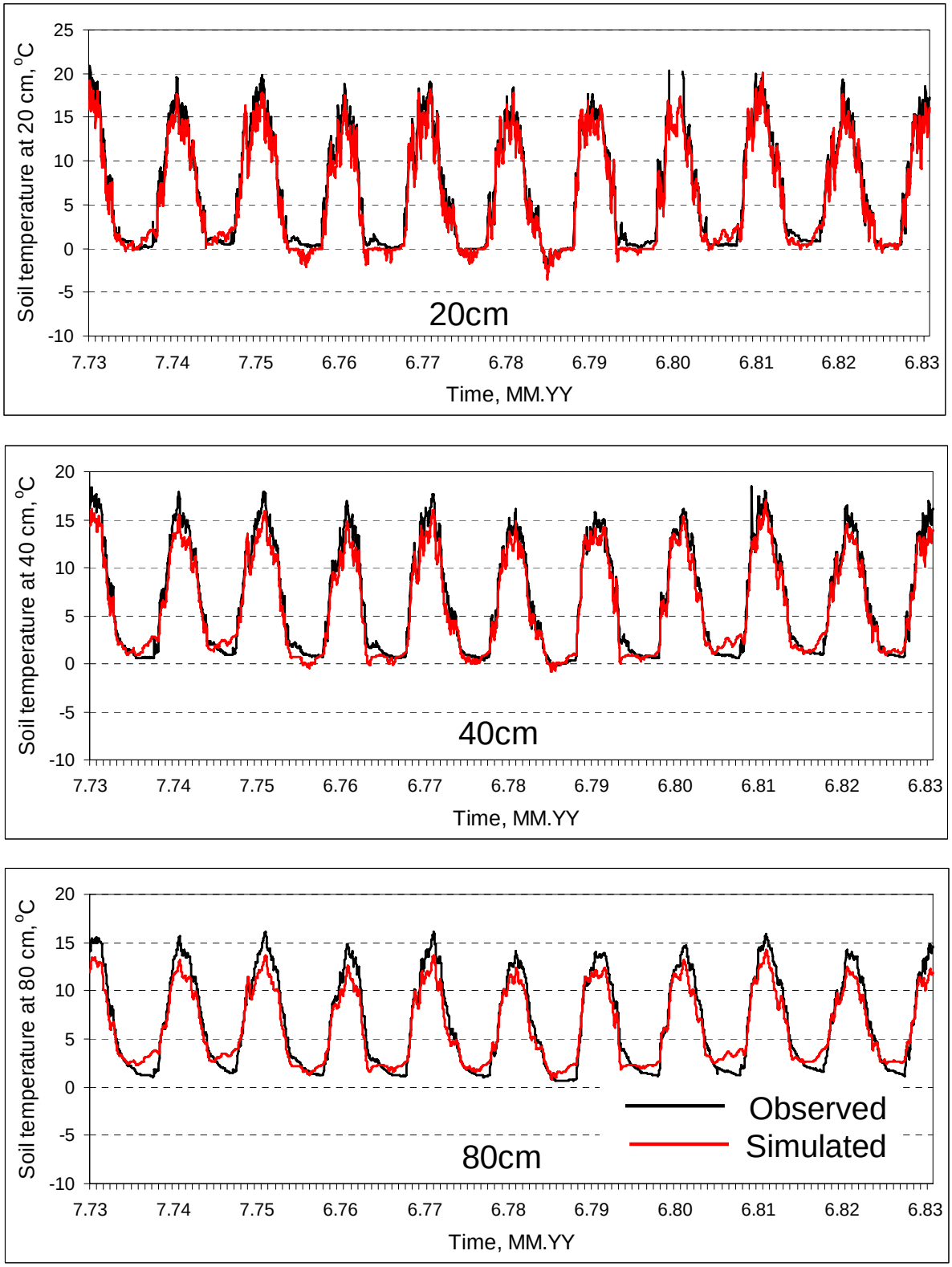

Figure 9b. Simulated and observed soil temperature, Valdai, Russia, at three depths: 20cm (top), 40cm (middle), and 80cm (bottom)

5.2 Basin Runoff tests

Complementing the point-type analyses, we further tested SAC-HT by generating multi-year streamflow simulations for eight river basins in Minnesota. SAC-HT was applied as a lumped model to the basins shown in Figure 5.

We first tested SAC-HT using *a priori* parameters without calibration. Output hydrographs at a 6-hr time step were generated from SAC-HT with the frozen ground component turned on and off. These 6-hr simulations were averaged to produce daily values for comparison against USGS observed mean daily flow values. Note, that SAC-HT has the same parameters as the original SAC-SMA. Therefore, the CONUS-wide *a priori* SAC-SMA parameters generated by Koren et al. (2003) from soil-vegetation data were used in this test.

Outlet hydrograph statistics from this test are shown in Table 4. It can be seen that the frozen ground version consistently outperforms the non-frozen ground version. Only 3 bias statistics of the 32 selected statistics became worse as a result using the SAC-HT with the frozen ground algorithm turned on. These results support the physical reasoning behind the frozen ground parameterization and the derivation of the *a priori* parameters.

To judge the impact of calibration on the simulation, we repeated these tests after calibrating the *a priori* soil parameters of the SAC-HT, the results of which are also shown in Table 4. Ten years of data were used in the calibration procedure, and the remaining 15-30 years of data were used for test purposes. The statistics in Table 4 were calculated for the entire 25-40 year period. As expected, calibration improves simulations, especially the total runoff bias.

Table 4. Comparison of simulation statistics with and without use of the SAC-HT frozen ground component for eight NCRFC basins from Table 2.

Statistics	*A priori* parameters		Calibrated Frozen ground version	*A priori* parameters		Calibrated frozen ground version
	W/o frozen ground	With frozen ground		W/o frozen ground	With frozen ground	
		RPDM5			LQPM5	
Daily RMSE, cms	17.36	16.13	15.50	11.95	11.51	8.32
Monthly RMSE, mm	9.67	9.15	8.49	7.93	7.56	4.65
Bias, %	2.01	3.76	-7.96	-9.85	-4.90	1.92
Correlation, R	0.83	0.86	0.90	0.72	0.75	0.86
		MMLM5			LNEM5	
Daily RMSE, cms	4.40	4.36	3.26	15.29	15.49	13.40
Monthly RMSE, mm	10.79	10.52	8.06	9.03	8.69	5.68
Bias, %	-23.90	-20.09	7.14	-44.96	-43.51	0.71
Correlation, R	0.68	0.69	0.84	0.66	0.65	0.72
		LGPM5			GRDM5	
Daily RMSE, cms	4.72	4.60	3.34	10.77	10.55	10.30
Monthly RMSE, mm	8.87	8.67	5.96	9.32	9.12	7.80
Bias, %	-43.32	-41.91	22.03	-5.36	-4.41	-6.13
Correlation, R	0.72	0.73	0.84	0.84	0.85	0.85
		DBCN8			AMEN8	
Daily RMSE, cms	2.70	2.55	2.14	1.71	1.63	1.57
Monthly RMSE, mm	4.70	4.37	3.23	8.23	7.09	5.99
Bias, %	62.79	75.35	-2.95	51.66	58.85	32.24
Correlation, R	0.61	0.67	0.77	0.57	0.64	0.67

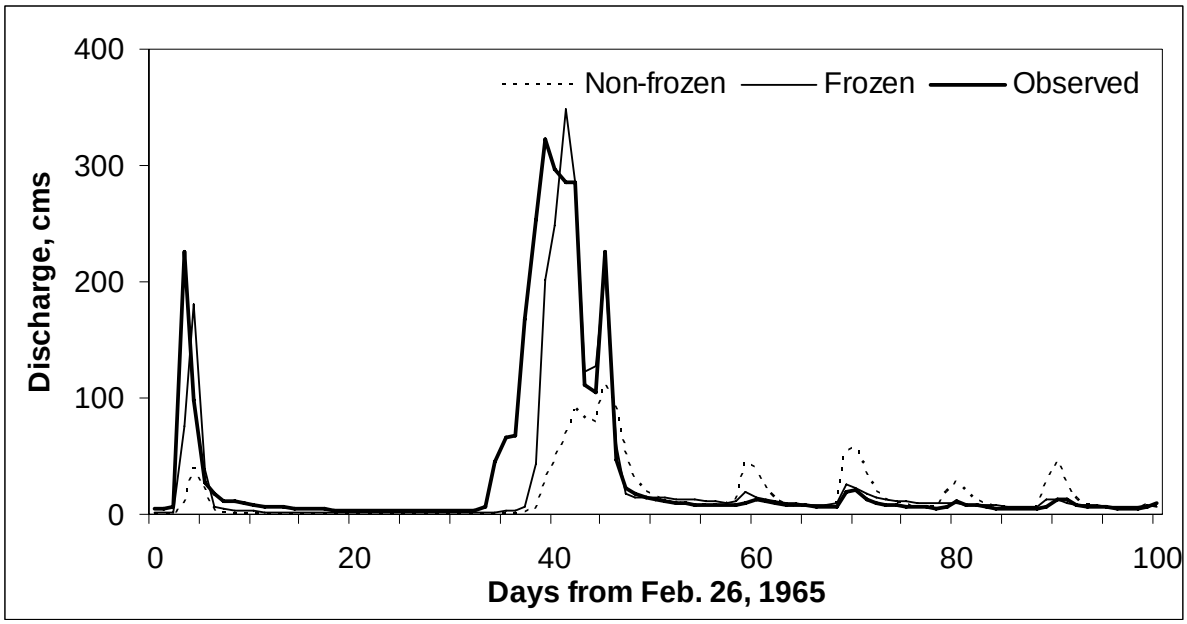

Figure 10. Effect of frozen ground on runoff dynamics. Simulation results from calibrated non-frozen and frozen ground versions of SAC-HT for basin LNEM5.

5.3 SAC-HT and Frost Depth

Frost depth can exert a strong influence on the runoff generation process. With this in mind, we also tested the ability of SAC-HT to compute frost depth. Observed frost depth data were obtained from the Wisconsin Snow and Frost Depth Report (Peterson et al., 1963). The map of frost depth given in the report is based on data collected from funeral directors and cemetery officials throughout Wisconsin. Figure 11 compares simulated and measured frost depth for the Root River basin. Considering that the Root River is about 100 km from the closest measurement point in Wisconsin, the match between the observed and simulated frozen depths is quite reasonable. SAC-HT was able to reproduce the deep frost depths which characterized the winters of 1966 and 1968, as well as very shallow frost depths of the 1967 and 1969 winters. An empirical estimate of the frost depth (frost index) based on the accumulated value of negative air temperature during the winter season also agrees well with the Wisconsin measurements (Peterson et al., 1963).

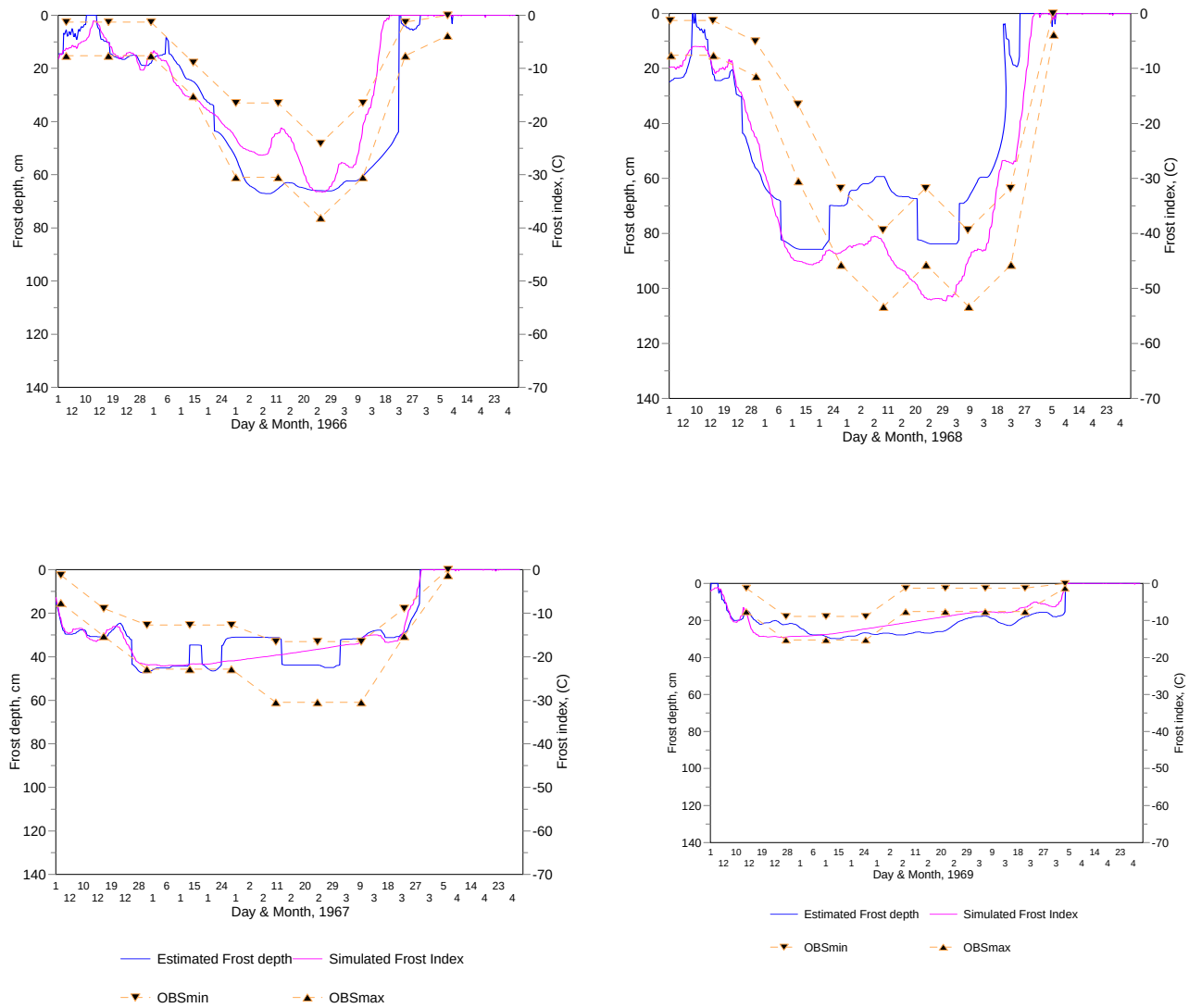

(Previous page) Figure 11. Comparison of simulated frost depth and frost index to measured frost depth for the Root River.

5.4 Regional soil moisture tests in the Oklahoma region

Gridded distributed modeling offers many advantages over traditional lumped modeling, and is seeing increased use both within the NWS and the research community. To assess SAC-HT's performance in this mode, the model was used to generate soil moisture estimates for 75 watersheds within the Arkansas-Red River basin in Oklahoma, as shown in Figure 7. These basins range in size from 20 km^2 to 15,000 km^2. SAC-HT was executed within the NWS Hydrology Laboratory Research Distributed Hydrologic Model (HL-RDHM; Koren et al., 2004) for a 7-year period at a 4 × 4 km grid using NEXRAD-based multi-sensor precipitation estimates. *A priori* soil-based SAC-SMA parameter grids over the CONUS (Koren et al., 2004) were used without any calibration. Rough estimates of channel and hillslope routing parameters from Koren et al. (2004) were applied to generate hydrographs at the selected watershed outlets.

Because of the minor effect of frozen ground in this region, the focus of this series of tests was not on SAC-HT's representation of frozen ground, but rather, on SAC-HT's ability to properly distribute soil moisture throughout the soil column. As such, the heat transfer component of SAC-HT was not 'turned on' in this test, meaning that water balance simulation results would be the same as from the original SAC-SMA model. However, SAC-HT was still used to compute the physically-based soil moisture estimates described in Section 3.2.2.2. Both Oklahoma-region grids and time series of basin average values of water balance components were generated. To ensure a proper comparison with the observed soil moisture data, SAC-HT soil moisture values in soil layers of variable thicknesses were recalculated into soil moisture at standard measurement depths. Initial results of these tests were presented in Koren et al. (2006). Here we will only discuss the results which highlight the advantages of the model modification as well as a potential problem with the soil water subtraction mechanism.

The model reproduces the basin average daily soil moisture dynamics well, with correlation coefficients between daily observed and simulated saturation ratios at the 0-25cm and 25-75 cm soil layers above 0.65 for most basins (Table 5). Overall basin-average correlation coefficients for the upper and lower soil layers are 0.79 and 0.75, respectively. Soil moisture simulation results also suggest that SAC-HT performs at a level equal to, or better than, two commonly used LSMs: Mosaic (Mitchell et al., 2004; Koster and Suarez, 1996) and Noah (Ek et al., 2003; Koren et al, 1999), Table 5. Because these two LSMs use different soil layer definitions, statistics were estimated at 0-5 cm, 0-25 cm and 25-75 cm for comparison with Noah, and at 0-10 cm and 10-40 cm for comparison with Mosaic. Simulations from Mosaic were available only for the period 10/1998 – 09/1999 and used a different forcing. Nonetheless, we include the comparison to Mosaic here for completeness. The SAC-HT statistics in Table 5 were calculated for the same period as the Mosaic simulation to enable a direct comparison. The Nash-Sutcliffe efficiency (NS) and root mean square error (RMSE) statistics are consistently better for SAC-HT than for the other two models. Correlation coefficients are higher for SAC-HT than for the other two models at the upper layers, but are lower in the deeper layer. Additionally, the SAC-HT simulation features a somewhat higher soil moisture bias. In terms of correlation, SAC-HT features good correlation between simulated and observed values of basin annual climatological soil

moisture: 0.70, 0.74, and 0.75 at 0-5 cm, 0-25 cm, and 25-75 cm respectively. The corresponding values from Noah are 0.68, 0.59, and 0.54, respectively.

The model-estimated climatological annual runoff at the basin outlets also agrees well with the measured runoff, and is characterized by a correlation coefficient of $R^2 = 0.92$. Both simulated and observed annual runoff values display a similar dependency on the basin wetness (Figure 12), expressed as a ratio of the mean annual precipitation to the potential evaporation (P/PE). A lower value of P/PE for a basin indicates the basin is dry while a higher value denotes the basin is wet.

Table 5. Daily soil moisture simulation results from SAC-HT, Noah, and Mosaic for Oklahoma Mesonet test basins.

Soil layer, cm	SAC-HT model				Land surface models			
	RMSE	Bias	R	NS	RMSE	Bias	R	NS
	01/1996 – 12/2002				Noah (01/1996 – 12/2002)			
0 - 05	0.109	-0.032	0.803	0.241	0.123	0.044	0.733	0.039
0 - 25	0.111	-0.031	0.794	0.238	0.117	-0.005	0.738	0.148
25 - 75	0.128	-0.077	0.746	-0.221	0.138	-0.092	0.827	-0.421
	10/1998 – 09/1999				Mosaic (10/1998 – 09/1999)			
0 - 10	0.127	0.088	0.770	-0.142	0.127	0.028	0.704	-0.169
10 - 40	0.116	-0.021	0.687	0.080	0.126	-0.011	0.701	-0.089

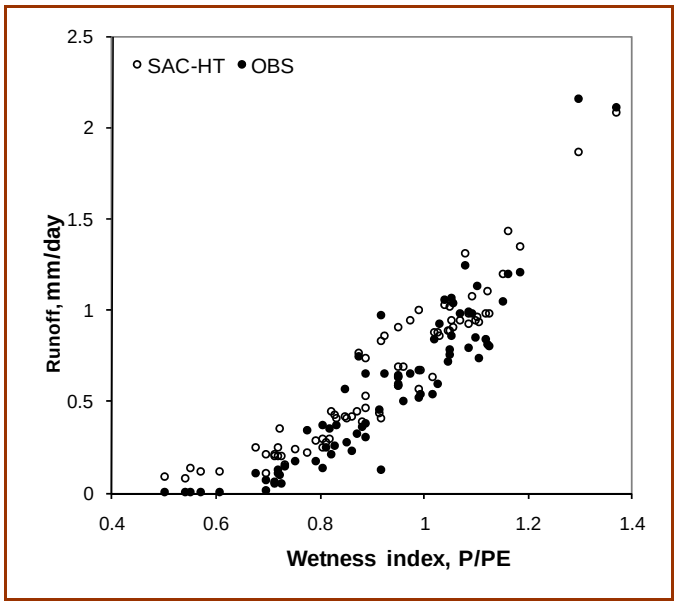

Figure 12. Simulated and observed climatological annual runoff vs. wetness index for test basins.

However, a closer look at the plot and at runoff at shorter time scales reveals the relatively weak performance of the model over very dry basins. This performance issue may be due, in part, to the way in which the SAC-HT *a priori* parameters were derived—using soil properties without explicitly accounting for climatological variables. Some studies, e.g.

Duan et al. (2001), suggest that climatological variables such as annual precipitation and potential evaporation exert considerable influence on the available soil water capacity. This variable plays a critical role in the derivation of the *a priori* parameters. Taking this into consideration, we applied a climate adjustment to two SAC-HT tension water parameters, the upper zone capacity, $S_{tmax,1}$, and lower zone capacity, $S_{tmax,2}$. To accomplish this, we used the climatological value of annual average greenness fraction as a climate index and adjusted both the upper and lower zone tension parameters with a power-type relationship:

$$S^*_{t\max,i} = S_{t\max,i} \cdot (c_i \cdot G_{avg}^{n_i} + d_i) \tag{14}$$

where G_{avg} is a climatological value of the annual average greenness fraction, index i varies from 1 to 2 indicating the upper or lower zone parameter*, and c, n*, and d are empirical parameters estimated based on limited calibration over 25 Mesonet basins; their values are: $c_1 = 0.62$, $d_1 = 0.193$, $n_1 = -0.579$ for the upper zone and $c_2 = 0.64$, $d_2 = 0.180$, $n_2 = -0.579$ for the lower zone. We applied this adjustment over the full extent of the CONUS *a priori* grids. Because Equation 14 is empirical in nature, we urge caution if it is applied outside of the specified range of the climate index ($0.2 \le G_{avg} \le 1.0$).

Another parameter that can affect model performance in dry regions is the percolation parameter, Z_{perc}. As formulated in SAC-HT, Z_{perc} can be estimated using the known maximum percolation rate, I_{max}:

$$Z_{perc} = \frac{I_{\max} - I_o}{I_o} \tag{15}$$

where I_o is the maximum base flow from the lower zone:

$$I_o = S_{f\max,2} \cdot r_2 + S_{f\max,3} \cdot r_3 \tag{16}$$

The original *a priori* Z_{perc} parameter definition is based on the assumption that the maximum percolation rate equals the maximum contents of the lower layer storages released over a certain time interval (Koren et al., 2002). However, it is not clear what time interval is appropriate. In the original version of the *a priori* parameter estimation, a 24 hour time interval was used. While this approach produces reasonable results in some areas, Z_{perc} values are often much lower than the values arrived at through manual calibration.

To improve the estimation of Z_{perc}, we utilize the Darcy-based infiltration equation (Appolov et al., 1974):

$$I(t) = K_s + \sqrt{\frac{K_s B \cdot D}{2t}} \tag{17}$$

where K_s is the saturated hydraulic conductivity, D is the soil moisture deficit, t is the time, and B is the water potential at the wetting front. As defined in SAC-HT, the maximum percolation rate from the upper layer occurs when the upper layer is filled and the lower layer is empty. Under these conditions, the water potential can be defined as a sum of the capillary potential (H) and the upper zone water depth $B=H+Z_U\cdot(\theta_{s,1}-\theta_{wlt,1})$, and the soil moisture deficit as the lower layer saturation reduced by the wilting point $D = \theta_{s,2} - \theta_{wlt,2}$.

To calculate the maximum percolation value, one needs to define a time interval in Equation 17. In this study, we define the time interval as the time elapsed during the steepest part of the infiltration curve of Equation 17. We select the point of maximum curvature of Equation 17 during the recession period as the end of this interval. At this point, the infiltration rate becomes close to a constant. We determined this point by first computing the equation of curvature of Equation 17. Setting the derivative of the curvature equation to zero and solving for t gives:

$$t_{\max} = \sqrt[3]{0.1K_s B \cdot D} \qquad \textbf{(18)}$$

Then the maximum percolation is an integral of Equation 17 over the time interval $\{0, t_{max}\}$:

$$I_{\max} = K_s t_{\max} + \sqrt{2K_s B \cdot D \cdot t_{\max}} \qquad \textbf{(19)}$$

We use Rawl's field data (Maidment, 1993) to define values of the capillary water potential H as shown in Table 6. Min-Max interval averages from Rawl's data for each soil type are assumed to be representative for that texture class.

Table 6. Rawl's minimum and maximum capillary water potential data

Texture class	Minimum H, mm	Maximum H, mm	Average, mm
Sand	10	254	130
Loamy sand	10	280	150
Sandy loam	30	450	240
Silt loam	30	950	490
Silt			550*
Loam	10	590	300
Sandy clay loam	40	1080	610
Silt clay loam	60	1310	680
Clay loam	50	910	480
Sandy clay	40	1400	710
Silt clay	60	1390	730
Clay	64	1560	810

Some uncertainty may arise when Equation 19 is applied to non-uniform soil profiles where the hydraulic conductivity differs greatly in the upper and lower zones. Based on sensitivity tests (not shown), we decided to use the lower zone hydraulic conductivity in instances where upper zone conductivity is greater than the lower zone values, and to use a two-zone average hydraulic conductivity when the upper zone conductivity is less than the lower zone value. Figure 13 shows the differences which occur over the CONUS between

the old and new *a priori* Z_{perc} percolation parameters. It confirms that the largest parameter differences occur in the drier western regions of the U.S. as expected. The new estimates of the percolation parameter agree much better with the calibrated values for a number of Oklahoma basins as shown in Figure 14.

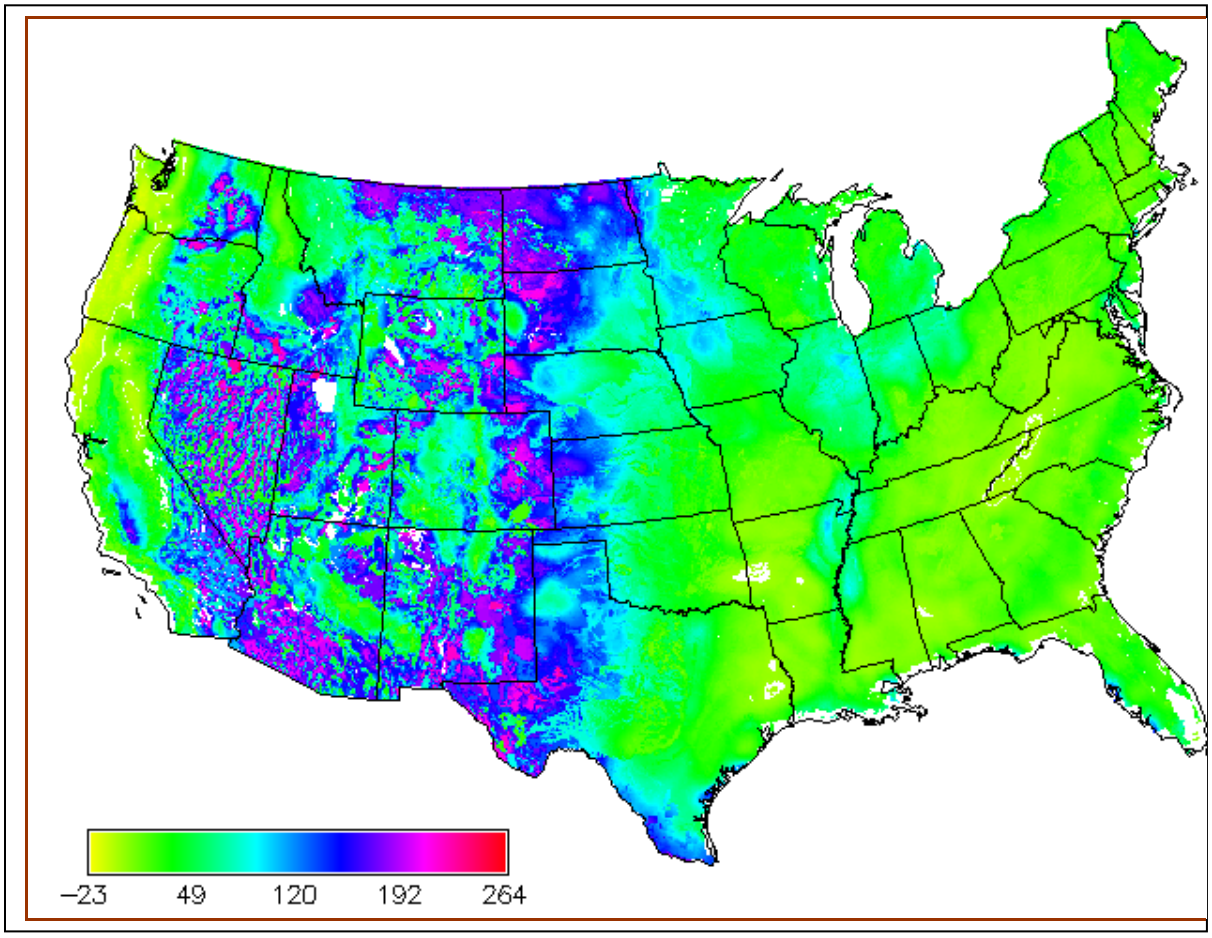

Figure 13. Differences between old and new gridded values of *a priori* Z_{perc} percolation parameter.

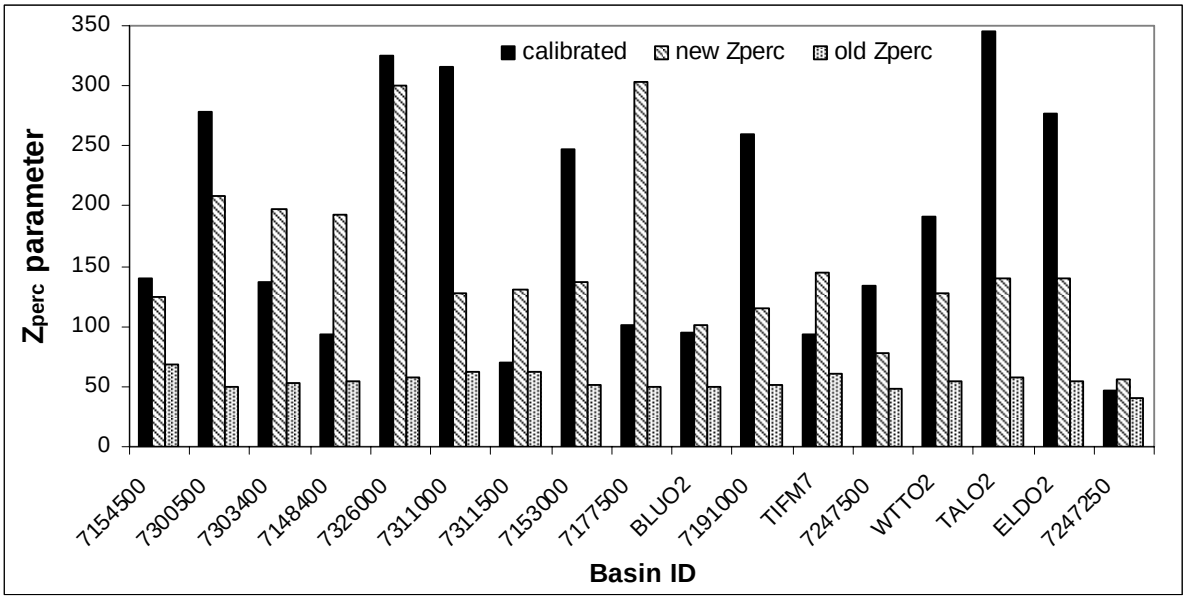

Figure 14. Comparison of calibrated Z_{perc} values to original (old) and climate-adjusted (new) Z_{perc} values.

5.4.1 Results using adjusted *a priori* parameters.

Echoing the experiments detailed in Koren et al. (2006), streamflow and soil moisture simulations were performed using the three climate-adjusted *a priori* parameter sets, $S_{tmax,1}$, $S_{tmax,2}$, and Z_{perc}. In these experiments, 40 uncalibrated Oklahoma Mesonet basins and 20 uncalibrated basins from the NWS West Gulf River Forecast Center test basins were added to the 25 calibrated Mesonet basins used in the climate adjustment derivation. Since the routing model parameters were not verified, daily or shorter time step comparisons were not performed. Instead, runoff statistics for all watersheds were calculated using a 10-day moving-average time series to reduce the effect of routing uncertainties. Upper and lower layer soil moisture statistics were estimated using daily data.

The average goodness of fit statistics for all basins are shown in Table 7, and it can be seen that use of the adjusted parameters leads to improved runoff statistics over both the calibrated and test (uncalibrated) basins.

In Figure 15, we present the improvement in runoff RMSE and Bias statistics gained by using the adjusted *a priori* parameters for the test basins. The %Improvement for these two statistics is computed as:

$$\%\text{RMSE improvement} = 100 \cdot (RMSE_{unadjusted} - RMSE_{adjusted}) / \overline{STD}_{obs} \quad (20)$$

$$\%\text{Bias improvement} = 100[abs(Bias_{unadjusted}) - abs(Bias_{adjusted})] / \overline{AVG}_{obs} \quad (21)$$

where $\overline{STD}_{obs}$ is the average standard deviation of the observed streamflow of all the test basins, and $\overline{AVG}_{obs}$ is the average of the observed values of all basins. As expected, the

greatest runoff improvement in both statistics is achieved for dry basins (i.e., smaller values of the climate index) as shown in Figure 15).

Table 7. Runoff and soil moisture statistics from adjusted *a priori* parameters compared to original unadjusted *a priori* parameters.

Version of Parameters	RMSE	Bias	AbsError	R
		Runoff, mm/day		
Adjusted	0.514	0.026	0.295	0.842
Unadjusted	0.578	0.089	0.329	0.834
		Upper layer soil moisture saturation, (0-25 cm)		
Adjusted	0.117	0.014	0.096	0.802
Unadjusted	0.113	-0.019	0.092	0.785
		Lower layer soil moisture saturation, (25-75 cm)		
Adjusted	0.124	-0.002	0.103	0.754
Unadjusted	0.127	-0.040	0.107	0.763

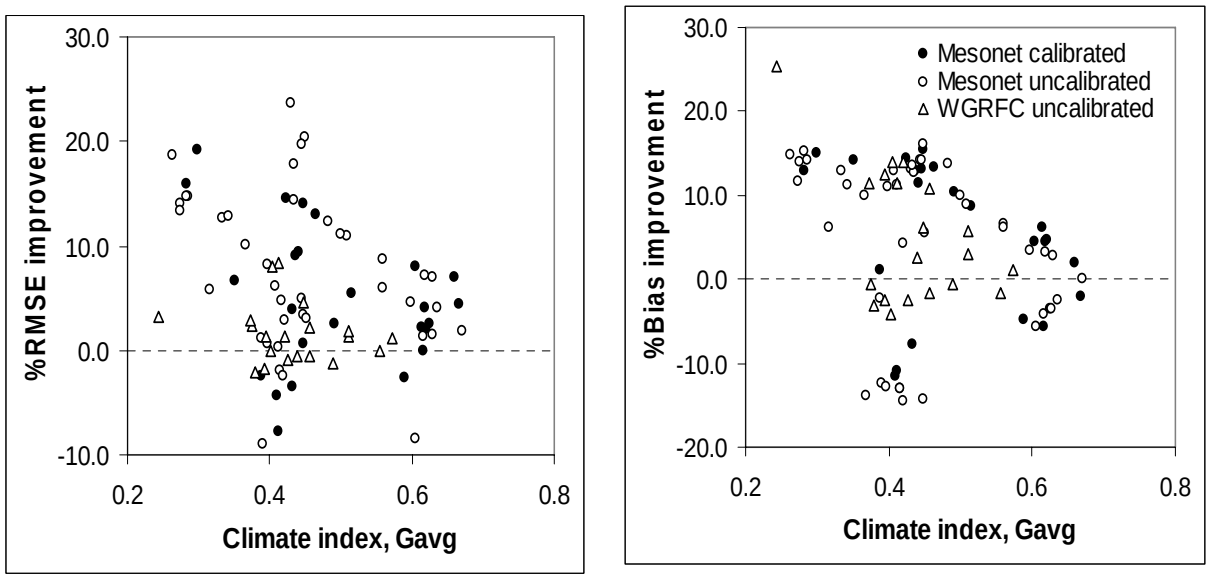

Figure 15. Runoff improvement statistics from adjusted *a priori* parameters compared to original *a priori* parameters.

There is also improvement in the soil moisture saturation bias for the both upper and lower soil layers. However, soil moisture RMSE and correlation coefficient improvements (changes) are minor. While RMSE at the lower layer slightly improves, the upper layer soil moisture RMSE slightly degrades; and the correlation coefficient is changed in the opposite direction. Similar to the runoff, there is more improvement of the lower layer RMSE for

drier basins as shown in Figure 16. However, there is no such trend for the upper layer accuracy.

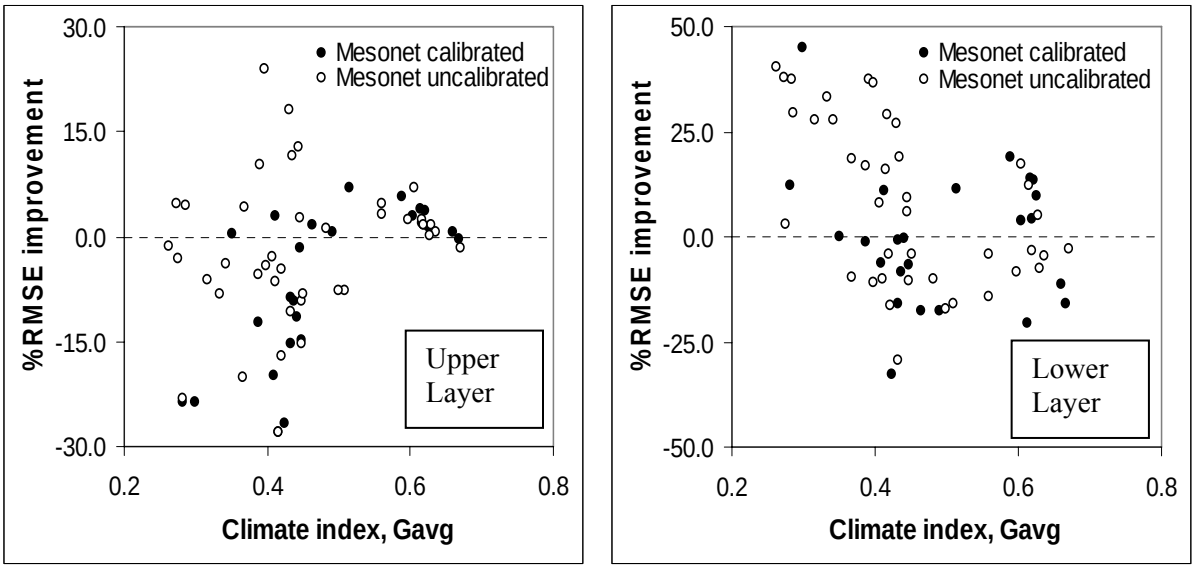

Figure 16. Improvement of the soil moisture saturation % RMSE from adjusted *a priori* parameters compared to original *a priori* parameters: upper soil layer (left panel) and lower soil layer (right panel).

A closer look at the seasonal variability of soil moisture suggests that use of climate adjusted parameters in simulations does not eliminate the underestimation of lower layer soil moisture, especially for very dry basins. While simulations of runoff are generally improved, the monthly climatological soil saturation of the lower layer is still much lower than that measured in the field. As an example, Figure 17 presents a typical case for dry region basins featuring a high percentage of bare soil and relatively deep grass roots. The plot depicts the runoff as well as the upper and lower layer soil moisture saturation ratios, and it can be seen that SAC-HT under-predicts the lower layer soil saturation for the January – June period. We believe that the most probable cause of this underestimation is a structural deficiency within the SAC-HT evapotranspiration component.

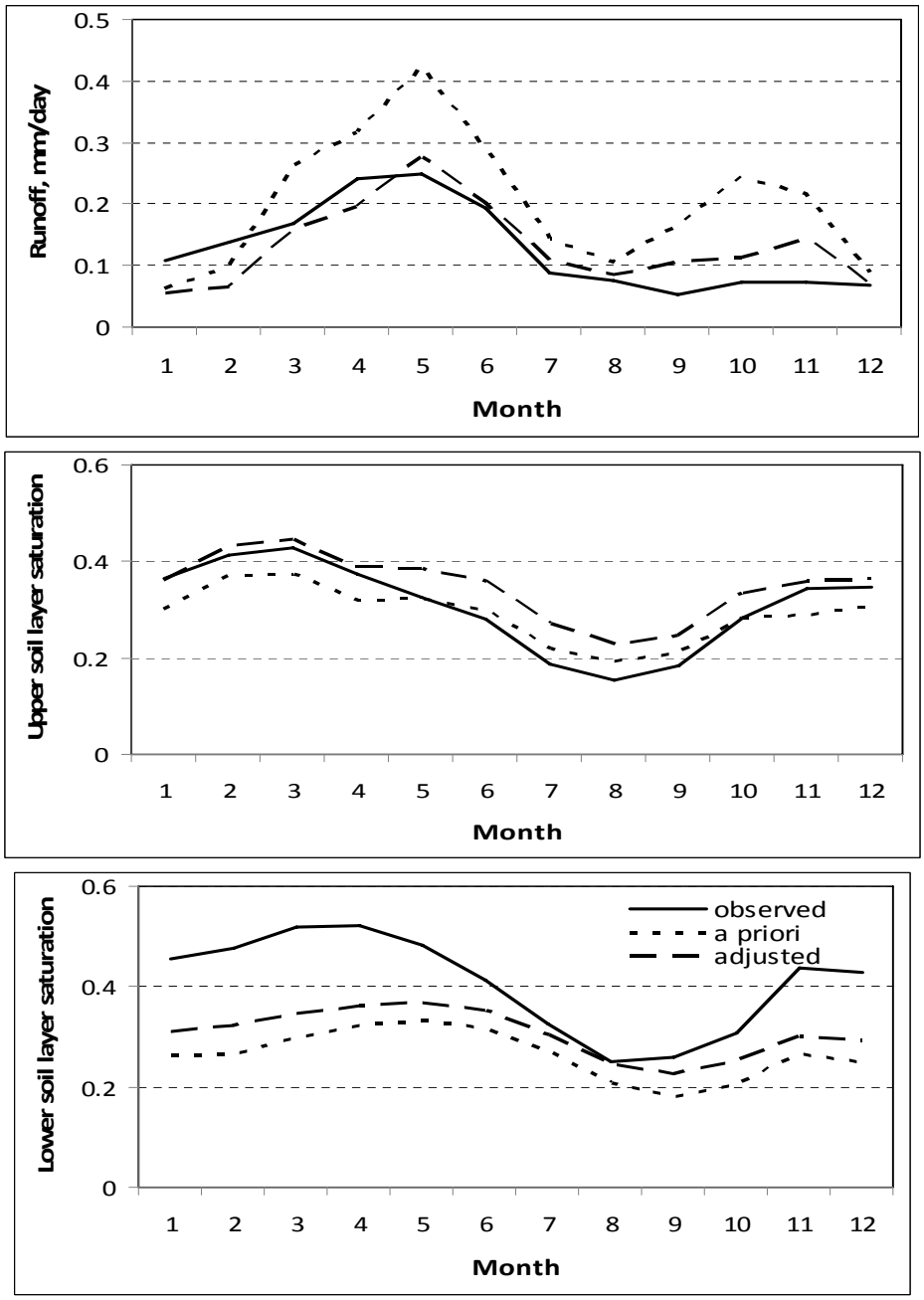

Figure 17. Comparison of monthly climatological runoff (top) and soil moisture estimated from measurements and model simulations for two layers using original and climate adjusted *a priori* parameters for basin 07325000 located in a dry area (climate index 0.34).

The evapotranspiration parameterization in SAC-HT (and its predecessor SAC-SMA) does not explicitly account for the effects of vegetation on the withdrawal of soil moisture. If the potential evaporation demand is not satisfied from the upper storage, the lower storages will supply water to fill this demand without regard to any actual physical connection between the upper and lower storages through vegetation or ground water. In reality, this linkage is critical for dry basins where the interaction between the upper and lower zones can

be broken for a prolonged period of time. In such cases, the subtraction of soil moisture from the lower zone should be satisfied mostly through the root zone. But, because SAC-HT does not have a specific root zone definition, its evapotranspiration component will lead to the disproportional removal of soil moisture from the upper and lower zones. For example, vegetation may respond to dry conditions by closing stomatal openings to reduce transpiration, a process which is not represented in SAC-HT. This problem will be addressed in the companion to this paper that focuses on the improvement of the evapotranspiration component of SAC-HT through incorporation of an explicit definition of the effects of vegetation on moisture extraction.

6. Conclusions and Discussion

We successfully modified the widely-used and well-established SAC-SMA hydrologic model to include a proven physically-based frozen soil algorithm. The frozen soil physics selected in this case was the algorithm of Koren et al., (1999). Li et al. (2010) classified this algorithm as one of medium complexity. Our work follows the recommendation of Robinson and Sivapalan (1995) that what was needed for the advancement of hydrologic prediction are connections between physics-based and conceptual models. The resultant model, SAC-HT, does not need calibration of the frozen ground component parameters. In this regard, SAC-HT satisfies the requirements discussed by Kirchner (2006) that a model 'gets the right answer for the right reason' without being over-parameterized and fitted to the calibration data. Moreover, this aspect has large implications for the operational forecasting community of the NWS and others. For the NWS, this new model can be implemented in place of the original SAC-SMA without the burden of additional calibration. The complexity of SAC-HT is commensurate with current and near-future operational meteorological forcings and application scales.

In addition to physically-based modeling of frozen ground effects, the SAC-HT can be used to generate gridded soil moisture and soil temperature estimates over CONUS. Indeed, the SAC-HT was executed at an hourly 4km scale over CONUS as part of the recent 30-year reanalysis NARR (Dong et al., 2011). Ongoing efforts in this re-analysis project will analyze a range of products from this 30 year run, including the derivation of soil moisture and soil temperature climatologies. Such climatologies could be used in conjunction with real time simulation of these variables to compute anomalies for water resources assessment and planning.

We performed numerous tests to evaluate the model's ability to simulate soil temperature, soil moisture, and the impacts on runoff of frozen soil across a wide variety of application scales and climatic regimes. These tests demonstrated the capability of SAC-HT to simulate soil moisture and temperature versus depth at point scales as well as runoff from many basins.

Climate adjustment to the *a priori* non-frozen ground parameters was required to correct for the overestimation of runoff and the underestimation of soil moisture in very dry basins and in lower soil layers. While this adjustment helped, it did not completely solve the underestimation of soil moisture in these instances. This development led us to identify a potential structural weakness in the SAC-HT (and SAC-SMA) evapotranspiration parameterization.

Our work represents a linkage of LSMs and hydrological models. The results

indicate that a path forward for water resources management can include the modification of precipitation/runoff models with physically-based components. While traditional hydrologic models often outperform LSMs in stream flow simulations (e.g. Smith et al., 2011; Gan et al., 2006; Reed et al., 2004), Hurkmans et al. (2008) suggest that LSMs contain the potential to more accurately estimate hydrological partitioning (evaporation, soil moisture, surface runoff and the streamflow) for two reasons. First, they derive evapotranspiration from coupled water and energy balance simulations rather than empirical or statistical methods to estimate evapotranspiration based on temperature. Second, they are able to utilize additional information provided by regional climate and weather models such as solar radiation, wind speed, specific humidity, etc. However, they caution that the complex model structure and the large number of parameters render LSMs generally more difficult to parameterize than hydrologic models.

The major recommendation from this study is to incorporate an advanced treatment of evapotranspiration into the SAC-HT model. This recommendation is addressed in the companion paper (Koren et al., 2011).

7. Acknowledgements

We are grateful to the organizers of the Oklahoma Mesonet for their assistance with the data for our study.

Appendix A: Derivation of Equations 7 and 8

Ground water release from a linear reservoir can be expressed as:

$$\frac{dS}{dt} = -(\alpha \cdot K_0) \cdot S \tag{A.1}$$

where S is reservoir water content, K_0 is the saturated hydraulic conductivity, and α is a constant that depends on soils and topographic properties. Integrating Equation A.1 under the assumption that groundwater level changes are small compared to the reservoir water content yields:

$$S_{t+\Delta t} = S_t \cdot e^{-\alpha \cdot \Delta t \cdot K_0} \tag{A.2}$$

where Δt is the integration time interval. The water release q per time interval can be expressed as:

$$q_{t+dt} = \frac{(S_t - S_{t+dt})}{\Delta t} = \frac{S_t \cdot (1 - e^{-\alpha \cdot \Delta t \cdot K_0})}{\Delta t} \tag{A.3}$$

From the SAC-SMA definition and Equations (7) and (5), the release rate r from unfrozen soil is defined as follows:

$$r = 1 - e^{-\alpha \cdot \Delta t \cdot K_0} \tag{A.4}$$

And the release rate r^* from frozen soil is:

$$r^* = 1 - e^{-\alpha \cdot \Delta t \cdot K_0 \cdot (1 + 8 \cdot \theta_f)^{-2}} \tag{A.5}$$

Substitution of Equation A.4 into Equation A.5 leads to the following relationship between the original SAC-SMA withdrawal rate and the frozen ground adjusted rate:

$$r^* = 1 - (1 - r)^{(1 + 8 \cdot \theta_f)^{-2}}$$

Appendix B: Relationship of Equations to Specific SAC-SMA Terminology

1. r_i is the generic term used in this report for the specific SAC-SMA withdrawal rate parmaters UZK and LZSK. UZK is the release rate from the Upper Zone Free Water storage and LZSK is the release rate from the Lower Zone Free Supplemental water storage.

2. Derivation of r_i:
   Assuming a linear reservoir water release
   $$\frac{dS}{dt} = -(\alpha \cdot K_0) \cdot S \tag{1}$$
   Solution of Eq. (1) is $S_{t+dt} = S_t \cdot e^{-\alpha \cdot \Delta t \cdot K_0}$ (2)
   water release per the time Δt
   $$q_{t+dt} = \frac{(S_t - S_{t+dt})}{\Delta t} = \frac{S_t \cdot (1 - e^{-\alpha \cdot \Delta t \cdot K_0})}{\Delta t} = \frac{S_i \cdot r_i}{\Delta t} \tag{3}$$

3. Derivation Eq. (x.2):
   From SAC-SMA definition $r_i = 1 - e^{-\alpha_i \cdot \Delta t \cdot K_{0.i}}$ (4)
   from (1) $e^{-\alpha_i \cdot \Delta t \cdot K_{0,i}} = 1 - r_i$ (5)
   adjusted $r_i^* = 1 - e^{-\alpha_i \cdot \Delta t \cdot K_{0.i} \cdot (1+8 \cdot \theta_f)^{-2}}$ (6)
   substitution Eq. (2) to (3) leads $r_i^* = 1 - (1 - r_i)^{(1-8 \cdot \theta_f)^{-2}}$ (7)

4. Definition in SAC-SMA parameters term
   Recalculation of interflow
   $$DUZ = 1 - (1 - UZK)^{DINC/(1+8 \cdot UZ_{ice})^2} \tag{8}$$
   where DUZ is the Recalculation of fast ground water flow
   $$DLZS = 1 - (1 - LZSK)^{DINC/(1+8 \cdot LZS_{ice})^2} \tag{9}$$
   Recalculation of percolation
   $$PERC = PERC \cdot \frac{1}{(1 + 8 \cdot UZ_{ice})^2} \tag{10}$$

9. References

Anderson, E.A., and Neuman, P., 1984. Inclusion of frozen ground effects in a flood forecasting model. Proceedings of the Fifth Northern Research Basins Symposium and Workshop, March 19-23, 1984, Vierumaki, Finland.

Anderson, E.A., 1976. National Weather Service River Forecast System, Snow Accumulation and Ablation Model, NOAA Technical Memorandum NWS HYDRO-17.

Anderson, E.A., 2006. Snow Accumulation and Ablation Model –SNOW-17. On-line documentation:
http://www.nws.noaa.gov/oh/hrl/nwsrfs/users_manual/part2/_pdf/22snow17.pdf

Appolov, B.A., G.P Kalinin, V.D. Komarov, 1974. Hydrological Forecasting (Kurs Gidrologicheskich Prognozov). Gidrometeoizdat, St. Petersburg (in Russian).

Basara, J.B., and Crawford, T.M., 2000. Improved installation procedures for deep-layer soil moisture measurements. Journal of Atmospheric and Oceanic Technology, Vol. 17, 879-884.

Brock, F.V., Crawford, K.C., Elliot, R.L., Cuperus, G.W., Stadler, S.J., Johnson, H.L., and Eilts, M.D., 1995. The Oklahoma Mesonet: A technical overview. Journal of Atmospheric and Oceanic Technology, Vol. 12, 5-19.

Burnash, R.J.C., Ferral, R.L., McGuire, R.A., 1973. A generalized streamflow simulation system conceptual model for digital computers, U.S. Department of Commerce National Weather Service and State of California Department of Water.

Carter, G.C. 2002. Infusing new science into the National Weather Service River Forecast System, 2nd Federal Interagency Hydrologic Modeling Conference, Las Vegas, Nevada, 10pp

Chen, F., Mitchell, K, Schaake, J., Xue, Y., Pan, H.-L., Koren, V., Duan, Q.Y., Ek, M., and Betts, A., 1996. Modeling of land surface evaporation by four schemes and comparison with FIFE observations. Journal of Geophysical Research, 101,7251-7268.

Cherkauer, K.A., Bowling, L.C., and Lettenmaier, D.P., 2003. Variable infiltration capacity cold land process model updates. Global and Planetary Change Vol. 38, 151-159.

Cherkauer, K.A., and Lettenmaier, D.P., 1999. Hydrologic effects of frozen soils in the Upper Mississippi River Basin. Journal of Geophysical Research, Vol. 104, No. D16, 19,599-19,610.

Clark, M.P., McMillan, H.K., Collins, D.B.G., Kavetski, D., and Woods, R., 2011. Hydrological field data from a modeller's perspective: Part 2: process-based evaluation of model hypotheses. Hydrological Processes, Vol. 25, 523–543, Published online 23 November 2010 in Wiley Online Library DOI: 10.1002/hyp.7902

Clark, M.P., Slater, A.G., Rupp, D.E., Woods, R.A., Vrugt, J.A., Gupta, H.V., Wagener, T., and Hay, L.E., 2008. Framework for understanding structural errors (FUSE): A modular framework to diagnose differences between hydrological models. Water Resources Research, Vol. 44, W00B02, doi:10.1029/2007WR006735

Duan, Q., Schaake, J., and Koren, V., 2001. *A priori* estimation of land surface model parameters. In: Lakshmi, V., et al. (Ed.) Land Surface Hydrology, Meteorology, and Climate: Observations and modeling Water Science and Applications 3. American Geophysical Union, Washington, D.C., pp 77-94.

Ek, M.B., Mitchell, K.E., Lin, Y., Rogers, E., Grunmann, P., Koren, V., Gayno, G., and

Tarpley, J.D., 2003. Implementation of Noah land surface model advances in the National Centers for Environmental Prediction operation mesoscale Eta model. Journal of Geophysical Research, Vol. 108, No. D22, 8851, doi:10:1029/2002JD003296.

Emerson, D.G., 1994. A Heat and Water Transfer Model for Seasonally Frozen Soils with Application to a Precipitation-Runoff Model. U.S. Geological Survey Water-Supply Paper 2389; available via USGS, Box 25286, MS 306, Federal Center, Denver Colorado.

Finnerty, B.D., Smith, M.B., Seo, D.-J., Koren, V., Moglen, G.E., 1997. Space-time sensitivity of the Sacramento model to radar-gauge precipitation inputs. Journal of Hydrology, Vol. 203, 21-38.

Illston, B.G., Basara, J.B., and Crawford, K.C., 2004. Seasonal to interannual variations of soil moisture measured in Oklahoma. International Journal of Climatology, Vol. 24, 1883-1896.

Illston, B.G., Basara, J.B., Fisher, D.K., Elliott, R., Fiebrich, C.A., Crawford, K.C., Humes, K., and Hunt, E., 2008. Mesoscale monitoring of soil moisture across a statewide network. Journal of Atmospheric and Oceanic Technology, Vol. 25, 167-182.

Koren, V.I., 2011. Physically based modifications to the SAC-SMA, Evapotranspiration component, NOAA NWS Technical Report 47,

Koren, V. I., 1980. Modelling of processes of river runoff formation in the forest zone of the European USSR. In: Soviet Meteorology and Hydrology, 78–85. Allerton Press, Inc., New York, USA.

Koren, V. Schaake, J., Mitchell, K., Duan, Q.Y., Chen, F., and Baker, J.M., 1999. A parameterization of snowpack and frozen ground intended for NCEP weather and climate models. Journal of Geophysical Research, Vol. 104, No. D16, 19,569-19,585.

Koren, V.I., Smith, M., Wang, D., Zhang, Z., 2000. Use of Soil Property Data in the Derivation of Conceptual Rainfall-Runoff Model Parameters. Proceedings of the 15th Conf. on Hydrology, AMS, Long Beach, CA, 103-116.

Koren, V., Smith, M., and Duan, Q., 2003. Use of a priori parameter estimates in the derivation of spatially consistent parameter sets of rainfall-runoff models. In: Duan, Q., Sorooshian, S., Gupta, H., Rosseau, A., and Turcotte, R., (Eds.) Advances in the Calibration of Watershed Models, Water Science and Applications Series, Vol. 6, AGU, Washington, D.C., pp 239-254.

Koren, V., Reed, S., Smith, M., Zhang, Z., Seo, D.-J., 2004. Hydrology laboratory research modeling system (HL-RMS) of the U.S. National Weather Service. Journal of Hydrology, Vol. 291, 297-318

Koren, V., 2006. Parameterization of frozen ground effects: sensitivity to soil properties. Predictions in Ungauged Basins: Promises and Progress (Proceedings of Symposium S7 held during the Seventh IAHS Scientific Assembly at Foz do Iquacu, Brazil, April 2005. IAHS Publication 303, 125-133.

Koster, R., and Suarez, M., 1996. Energy and water balance calculations in the Mosaic LSM, NASA Technical Memorandum, Vol. 9, 60pp.

Kozeny, J., 1927. Ueber kapillare Leitung des Wassers im Boden. Sitzungsber Akad. Wiss., Wien, 136(2a), 271-306.

Kulik, V.Y., 1969. Effects of ice content on the soil conductivity. Meteorology and

Hydrology, No 9, 66-71, (translated from Russian).
Kulik, V.Y., 1978. Water infiltration into soil (in Russian). Gidrometeoizdat, Moscow, 19878, 93pp
Larson, L.W., Ferral, R.L., Strem, E.T., Morin, A.J., Armstrong, B., Carroll, T.R., Hudlow, M.D., Wenzel, L.A., Schaefer, G.L., and Johnson, D.E., 1995. Operational Responsibilities of the National Weather Service River and Flood Program, Weather and Forecasting, Vol. 10, 465-476.
Li, Q., Sun, S., and Y. Xue, Y., 2010. Analyses and development of a hierarchy of frozen soil models for cold region study, Journal of Geophysical Research, 115, D03107, doi:10.1029/2009JD012530
Liang, X., Lettenmaier, D.P., Wood, E.F., 2006. One-dimensional Statistical Dynamic Representation of Subgrid Spatial Variability of Precipitation in the Two-Layer Variable Infiltration Capacity Model, J. Geophys. Res., 101(D16) 21,403-21,422, 1996.
Luo, L, Robock, A., Vinnikov, K.Y., Schlosser, C.A., Slater, A.G., and others, 2003. Effects of Frozen Soil on Soil Temperature, Spring Infiltration, and Runoff: Results from the PILPS 2(d) experiment at Valdai, Russia. Journal of Hydrometeorology, Vol. 4, 334-351.
Maidment, D. R., 1993. Handbook of Hydrology. McGraw-Hill Professional, 1424 pp.
McEnery, J., Ingram, J., Duan, Q., Adams, T., and Anderson, L., 2005. NOAA'S Advanced Hydrologic Prediction Service – Building pathways for Better Science in Water Forecasting. Bulletin of the American Meteorological Society, March, 375-385.
Mitchell, K.E., et al., 2004. The multi-institutional North American Land Data Assimilation System (NLDAS): Utilizing multiple GCIP products and partners in a continental distributed hydrological modeling system. Journal of Geophysical Research, Vol. 109, D07S90, doi:10.1029/2003JD003823.
Mitchell, K., Ek, M., Lohmann, D., Koren, V., Schaake, J., Duan, Y., Grunmann, P., Gayno, G., Lin, Y., Rogers, E., Tarpley, D., and Peters-Lidard, C., 2002. Reducing near-surface cool/moist biases over snowpack and early spring wet soils in NCEP Eta model forecasts via land surface model upgrades, 16th Conference on Hydrology, January, 2002, Orlando, FL, AMS, paper J1.1, pp. J1-J6.
Mou, L., Tian, F., Hu, H., and Sivapalan, M., 2008. Extension of the representative elementary watershed approach for cold regions: constitutive relationships and an application. Hydrology and Earth System Sciences, Vol. 12, 565-585
Nash, J.E., Sutcliffe, J.V., 1970. River flow forecasting through conceptual models. Part I, a discussion of principles. Journal of Hydrology Vol. 10, 282-290.
Niu, G.-Y., and Yang, Z.,-L, 2006. Effects of frozen soil on snowmelt runoff and soil water storage at a continental scale. Journal of Hydrometeorology, Vol. 7, 937-952.
Peterson, A.E., Burley, M.W., and Caparoon, C.D., 1963. Frost Depth Survey: A New Approach in Wisconsin, revised from Weatherwise, April 1963.
Reed, S., Koren, V., Smith, M., Zhang, Z., Moreda, F., Seo, D.-J., DMIP Participants, 2004. Overall distributed model intercomparison project results. Journal of Hydrology, Vol. 298, Nos. 1-4, 27-60.
Reed, S., Schaake, J., Zhang, Z., 2007. A distributed hydrologic model and threshold frequency-based method for flash flood forecasting at ungauged locations. Journal of Hydrology, Vol. 337, 402– 420.
Robinson, J.S., and Sivapalan, M., 1995. Catchment-scale runoff generation model by aggregation and similarity analysis. In: Kalma, D..D., Sivapalan, M. (Eds.), Scale

Issues in Hydrological Modeling. Wiley, New York, 311-330.
Roe, J., Dietz, C., Restrepo, P., Halquist, J., Hartman, R., Horwood, R., Olsen, R., Opitz, H., Shedd, R., and Welles, E., 2010. NOAA's Community Hydrologic Prediction System. Paper 7B.3 Proceedings of the 26th Conference on Interactive Information and Processing Systems (IIPS) for Meteorology, Oceanography, and Hydrology, AMS
Schneider, J.M., Fisher, D.K., Elliott, R.L., Brown, G.O., and Bahrmann, C.P., 2003. Spatiotemporal variations in soil water: First results from the ARM SGP CART network. Journal of Hydrometeorology, Vol. 4, 106-120.
Schlosser, C.A., Robock, A., Vinikov, K.Y., Speranskaya, N.A and Xue, Y., 1997. 18-Year land-surface hydrology model simulations for a midlatitude grassland catchment in Valdai, Russia. Monthly Weather Review, Vol. 125, 3279-3296.
Smith, M., Koren, V., Zhang, Z., Zhang, Y., and DMIP 2 participants, 2011. Results of the Oklahoma DMIP 2 experiments. Journal of Hydrology, in review.
Taylor, G.S., and J.N. Luthin, 1976. Numeric results of coupled heat-mass flow during freezing and thawing. The 2nd Conference on Soil Water Problems in Cold Regions, Natural Resources Council, Edmonton, Alberta, Canada, September 1-2.
Tian, F., Hu, H., Lei, Z., and Sivapalan, M., 2006. Extension of the representative elementary watershed approach for cold regions via explicit treatment of energy related processes. Hydrology and Earth System Science, Vol. 10, 619–644.
Vinnikov, A., Robock, A., Speranskaya, N.A., and Schlosser, C.A., 1996. Scales of temporal and spatial variability of mid-latitude soil moisture. Journal of Geophysical Research, Vol. 101, 7163-7174.
Wang, L., Koike, T., Yang, K., Jin, R., and Li, H., 2010. Frozen soil parameterization in a distributed biosphere hydrological model. Hydrologic and Earth System Sciences, Vol. 14, 557-571.
Wang, A., Li, K.Y., and Lettenmaier, D.P., 2008. Integration of the variable infiltration capacity model soil hydrology scheme into the community land model. Journal of Geophysical Research, Vol. 113, DO9111, doi:10/1029/2007JD009246.
Xia, Y., Mitchell, K., Ek, M., Cosgrove,B., Sheffield, J., Luo, L., Alonge, C., Wei, H., Meng, J., Livneh, B., Duan, Y., and Lohman, D., 2011a. Continental-Scale Water and Energy Flux Analysis and Validation for North-American Land Data Assimilation System Project Phase 2, Part 1: Intercomparison and Application of Model Products, Journal of Geophysical Research, submitted.
Xia, Y., Mitchell, K., Ek, M., Cosgrove, B., Sheffield, J., Luo, L., Alonge, C., Wei, H., Meng, J., Livneh, B., Duan, Y., and Lohman, D., 2011b. Continental-Scale Water and Energy Flux Analysis and Validation for North-American Land Data Assimilation System Project Phase 2, Part 2: Validation of Model-Simulated Streamflow. Journal of Geophysical Research, submitted
Zhang, X., Sun, S.F., and Xue, Y., 2007. Development and testing of a frozen soil parameterization for cold region studies. Journal of Hydrometeorology, Vol. 8, 690-701.